AFML-TR-70-83

HOLE GROWTH IN THIN PLATES PERFORATED BY HYPERVELOCITY PELLETS

W. C. Turpin
University of Dayton
Research Institute

and

J. M. Carson, Captain, USAF
Air Force Materials Laboratory

Air Force Materials Laboratory
Air Force Systems Command
Wright-Patterson Air Force Base, Ohio

NOTICES

When Government drawings, specifications, or other data are used for any purpose other than in connection with a definitely related Government procurement operation, the United States Government thereby incurs no responsibility nor any obligation whatsoever; and the fact that the Government may have formulated, furnished, or in any way supplied the said drawings, specifications, or other data, is not to be regarded by implication or otherwise as in any manner licensing the holder or any other person or corporation, or conveying any rights or permission to manufacture, use, or sell any patented invention that may in any way be related thereto.

This document has been approved for public release and sale; its distribution is unlimited.

Copies of this report should not be returned unless return is required by security considerations, contractual obligations, or notice on a specific document.

AFML-TR-70-83

HOLE GROWTH IN THIN PLATES PERFORATED BY HYPERVELOCITY PELLETS

W. C. Turpin
University of Dayton
Research Institute

and

J. M. Carson, Captain, USAF
Air Force Materials Laboratory

FOREWORD

This report covers research performed on the Air Force Materials Laboratory light-gas gun facility. Some of the individual tasks covered in this report were carried out by AFML personnel while the remainder were pursued by the University of Dayton Research Institute, Dayton, Ohio, under Air Force Contract F33615-68-C-1138. The contract was initiated under Project 7360, "Chemical, Thermal, and Dynamic Properties of Materials", Task 736006, "Response of Materials to Impulsive Loading". The work was administered by the Air Force Materials Laboratory, Air Force Systems Command, Wright-Patterson AFB, Ohio with Mr. Gordon Griffith (MAYH) as Project Engineer.

The authors gratefully acknowledge the assistance of Mr. H. F. Swift for his helpful discussion and advice and Mr. H. R. Taylor and Mr. E. A. Strader for their technical assistance and support.

This report was submitted by the authors in April 1970. The University of Dayton report number is UDRI-TR-70-16.

This technical report has been reviewed and is approved.

HERBERT M. ROSENBERG
Chief, Exploratory Studies Branch
Materials Physics Division
Air Force Materials Laboratory

ABSTRACT

An experimental study has measured hole growth rates in thin plates impacted by hypervelocity pellets. These hole growth rates were obtained for 0.85 mm thick plates made of aluminum, copper, and cadmium impacted at 5-7 km/sec with 3.18 mm spheres of like material. The growth process was found to be a two stage process. Results are compared with the numerical predictions from a two dimensional impact code. These dynamic results are combined with observations resulting from a catalog of over 400 hole corpse measurements to form a qualitative model of thin plate impact.

CONTENTS

LIST OF ILLUSTRATIONS

List of Illustrations (Continued)

LIST OF TABLES

LIST OF SYMBOLS

D_D = hole diameter at time t

D_F = final hole diameter

t = time after impact

ρ_t = target density

ρ_p = pellet density

d = pellet diameter

t_s = plate thickness

V = impact velocity

C = material sonic velocity

ε = ultimate room temperature tensile strain in percent

I. INTRODUCTION

Protection of structures from hypervelocity particle impact either of meteoroid or man made origin, is a continuing requirement of our aerospace program. For this reason, the spaced bumper concept of hypervelocity particle protection, first proposed by Whipple in 1946[1], has been developed. It consists of a thin* sacrificial shield mounted some distance from the main structure surface. The incoming particle shatters as it perforates this shield. As a result, a diffuse cloud of debris impacts the main surface. Figure 1 presents a sequence of high speed photographs of a debris cloud of this type generated in the laboratory. The cloud produces a much less severe point loading condition on the surface of a shielded structure than would exist with the direct impact of the original particle. Efficiencies as high as a factor of eight in total thickness of material required to resist perforation can be realized with optimal shield designs[2]. In order to maximize the potential weight savings, then, it becomes essential to understand spaced shield operation. Specific areas include the hypervelocity perforation process in thin plates, and the makeup of the subsequently generated debris clouds. This type of information is also necessary to any meaningful prediction of potential perforation damage to single sheet structures exposed to impact environments.

The damage potential of a thin plate impact can be broken into two categories, one associated with the actual hole formed in the impacted plate and the other with the lethal cloud of debris generated to the rear of the plate. The size of a perforation affects the decompression rate of a punctured pressure vessel--up to and including catastrophic structural failure from running cracks triggered by hole formation. The cloud of energetic debris behind the impacted plate, although distributed over a relatively large area, still has the potential to disrupt any surface it intercepts. Prediction of the effects and extent of this type of damage requires a quantitative knowledge of the thin plate impact process and associated effects. Information pertaining to the debris cloud (such as shape, material distribution, velocity profile, etc.) can be related to the hole formation process. A detailed study of hole growth offers an approach whereby the dual damage mechanisms associated with thin plate impact can be investigated.

---

* Thin as used in this report is qualitatively defined as a plate thickness that will be completely perforated by the primary penetrating effects of the impacting design meteoroid and result in identical entrance and exit hole structure.

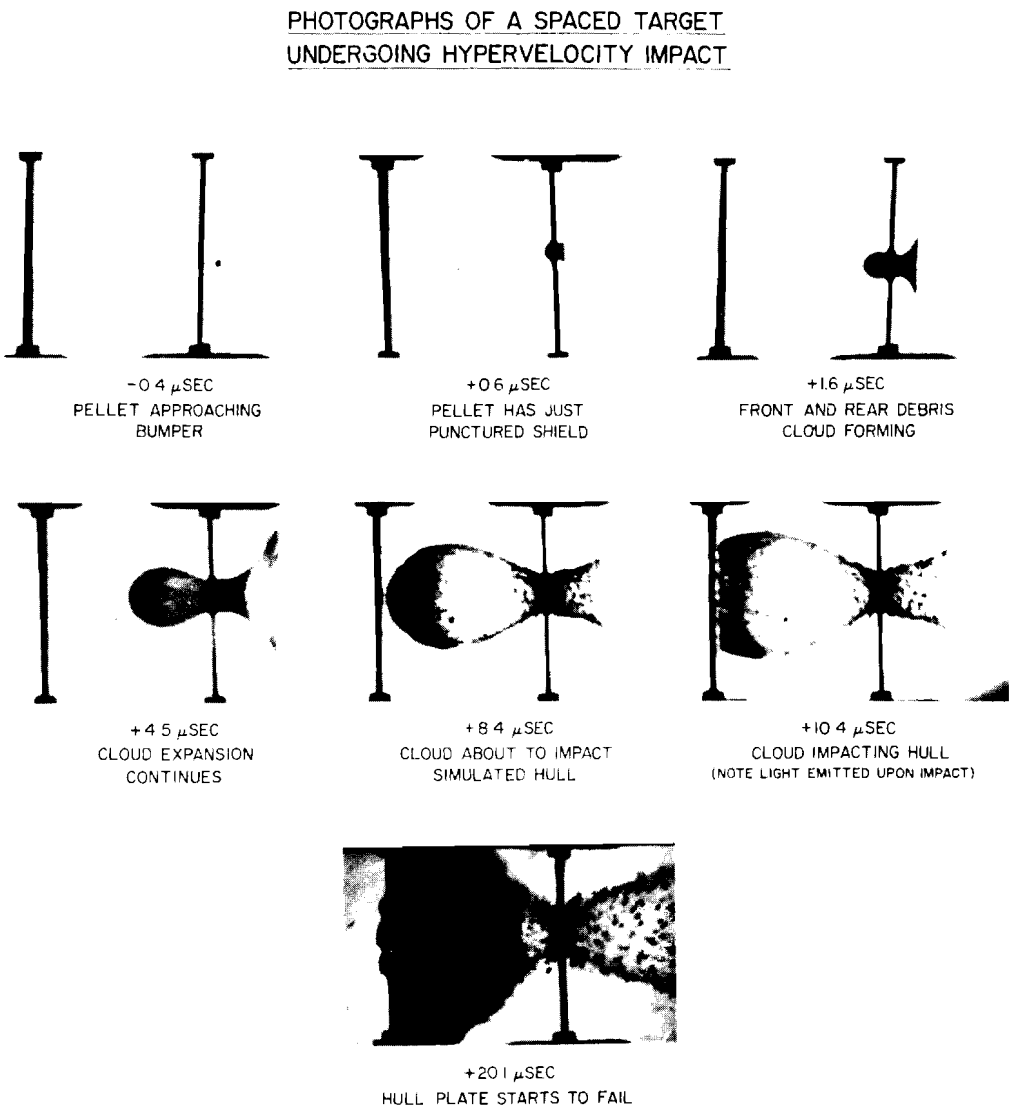

Figure 1. Hypervelocity Impact on a Spaced Bumper-Hull Combination

A second, and perhaps more fundamentally important aspect of hole formation studies, is the acquisition of a data base from which a better understanding of basic hypervelocity impact phenomena can be derived. The thin plate impact case presents the most basic situation for analysis since the bulk of the high energy material is projected away from the vicinity of impact before pressures drop to the point where material strength effects become important. Analysis of this case should allow certain simplifying assumptions about materials response to applied stresses not permissible under most impact conditions and yet lead to conclusions applicable to all hypervelocity impact situations. Hole growth, then, is an important key to a more complete understanding of hypervelocity impact from the standpoints of both engineering and fundamental research.

As part of an overall effort to characterize the nature of and understand the mechanisms behind hypervelocity impact into both thin sheets and semi-infinite targets the Air Force Materials Laboratory has conducted a precise dynamic study of hole growth in impacted thin plates. This work is combined in this report with a large body of post-mortem hole measurements in plates of various thicknesses and materials impacted by a variety of hypervelocity pellets.

II. DYNAMIC HOLE GROWTH

The dynamic study of hole growth presented here is an extension of an earlier effort[3]. Emphasis, during this study was placed on early-time hole growth, with enough data points at later times to assure synchronization of the old and new data. A pellet diameter to target thickness ratio of four was used, as before, in order to generate maximum average impact pressures[4].

Hole growth curves were obtained for 0.85 mm thick plates made of 6061-T6 aluminum, OFHC copper, and commercially pure cadmium impacted with 3.18 mm diameter pellets of the same materials. To provide the possibility of examining size scaling effects, one additional series of firings of 6.36 mm diameter pellets into 1.70 mm thick plates was made. Each of the resulting experimental curves, with the exception of the latter, was compared with a numerical prediction of hole growth rate from a two dimensional impact code applied to nominally identical impact situations[5]. This particular code (STEEP)* is based on hydrodynamic approximations and includes factors to account for material strength effects. Finally, dynamic debris cloud data from previous AFML studies[3, 6] was re-examined in conjunction with the new hole growth curves.

Experimental Procedure

Hole growth data was collected by taking short duration radiographs ($\sim$ 30 nsec) of the target plate at various predetermined times after initial pellet-target contact. Six flash x-ray tube heads** were mounted in an approximately circular array behind the target tank and each was aimed at the impact point of the mounted target plate (see Figure 2). X-ray shadow images of the growing hole in the target were impressed on film in a standard x-ray cassette mounted 15 cm uprange from the target. A 2.5 cm hole in this cassette was required to provide for passage of the pellet to the target plate. Finally, a 6 mm thick lead mask was mounted immediately behind the target plate with a 5 cm hole in it centered on the pellet trajectory to prevent x-rays emitted by one source from fogging images of another.

The basic instrumentation circuit is diagramed in Figure 3 with the exception that 6 instead of 5 x-ray channels were used in the actual experiment. Flow is from left to right. Two orthogonally positioned image

---

* STEEP is the two-dimensional Eulerian elastic-plastic code of Shock Hydrodynamics, Inc.

** Field Emission Fexitron Model 231 and 154 Systems.

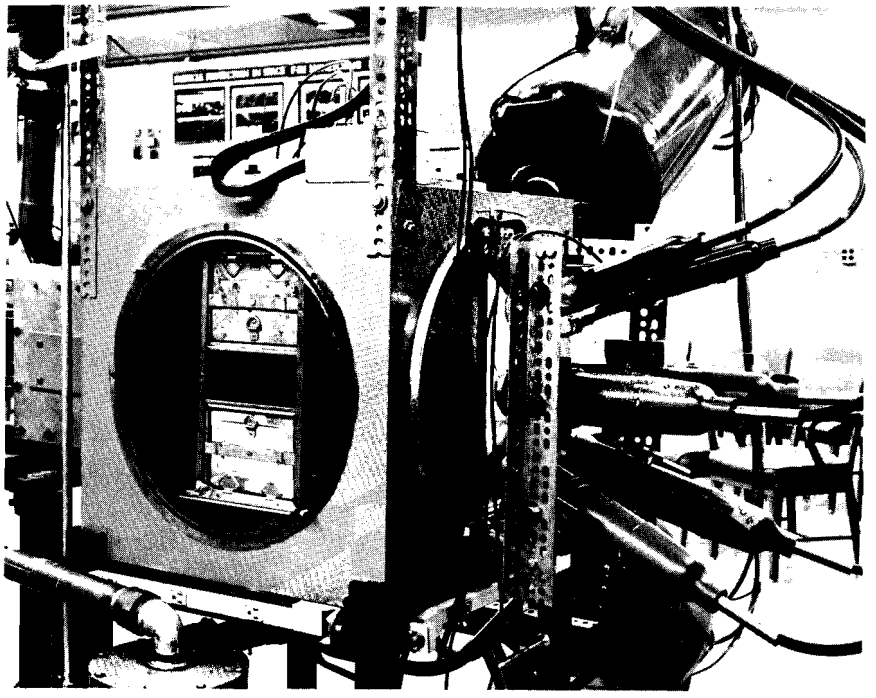

Figure 2. X-ray Heads in Mounted Position on Rear of Target Tank

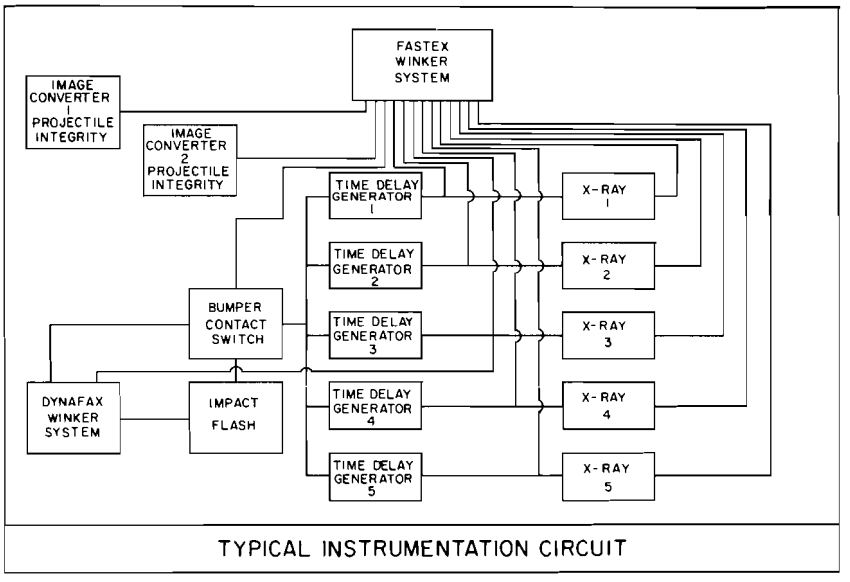

Figure 3. Radiograph Instrumentation Circuit

converter cameras* verified the pellet integrity prior to its entrance into the target tank. A thin Mylar/foil sandwich switch mounted either on the target face or at a small standoff was used to generate a trigger signal when punctured by the pellet. This signal was fed through time delay generators to each of the x-ray generators. With this technique, the sequential firing rate of the x-ray heads could be adjusted at will and the malfunction of any time delay would cause the loss of only one radiograph.

The precise firing times of individual x-rays were determined by two independent means. The breakdown of voltage stressed gap switches mounted on each x-ray tube head[7] was used to trigger small xenon flash tubes that were viewed by a reel type streaking camera**. In addition, small 6.0 to 12.0 mm long thallium doped, sodium iodide crystals were placed slightly off axis on each x-ray tube head. These crystals generate high intensity, short rise-time light flashes when subjected to an intense x-ray flux. As long as the crystals were mounted to intercept only the periphery of the central flux cone, they did not interfere with the generation of an x-ray film image of the growing hole. Optical fibers from crystals mounted in the beams of each x-ray head were arranged in a single linear array that was viewed by a rotating drum streak camera*** where the relative times between crystal excitation (and hence x-ray pulses) were displayed as image displacements along the direction of film motion. The fiber array also included optical fibers set to view impact flash and to view a xenon flash tube triggered by the original Mylar/foil sandwich switch so that the x-ray burst times could be related to impact time. A schematic of this system is shown in Figure 4.

Experimental Results

The primary information derived from dynamic hole growth experiments was hole size versus time data (see Table I). Tabulated results for the three materials in the standard configuration and aluminum in the scaled up configuration are presented in Tables II through V. Figures 5 through 8 depict the normalized data points graphically and are each paired with the appropriate table. Note that different graphing symbols represent different shots. The graphs are all drawn to the same scale to facilitate comparison. In addition, they include a curve representing the least squares fit of the data to a prony series curve. This series has the form

$$y = \sum_{i=0}^{i} A_i e^{B_i X}$$

---

* Beckman & Whitley Model 500 Image Converter Camera.

** Wollensak 16 mm Oscillographic Camera.

*** Beckman & Whitley Model 319B Streaking Camera.

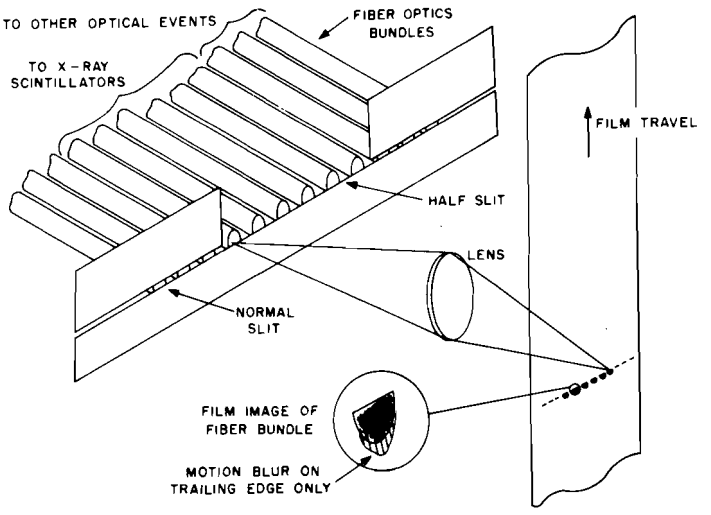

Figure 4. Schematic of Scintillation Crystal Streak Recording Technique

Table I

Experimental Program

Material	Proj. Dia. (mm)	Plate Thickness (mm)	Hole Dia. (mm)	Vel. $\frac{km}{sec}$	Shot No.
Al	3.18	0.85	6.96	7.32	2397
			6.96	7.23	2398
			6.96	7.23	2399
			6.97	7.23	2400
			6.78	7.06	2705
			6.79	7.02	2706
			13.55	6.98	2714
			13.27	6.74	2715
Cu	3.18	0.85	8.38	7.14	2393
			8.27	7.06	2394
			8.39	7.25	2396
			8.28	6.98	2709
			8.59	6.93	2717
Cd	3.18	0.85	9.62	7.19	2710
			9.76	7.04	2716

Table II

Al-Al Hole Growth at 7 km/sec*

Shot No.	Time (μsec)	$D_D/D_F \left(\frac{\text{Dia During}}{\text{Dia Final}}\right)$
2397	10.35 ± 0.50	1.025 ± 0.03
	11.43 ± 0.50	1.022 ± 0.03
	12.50 ± 0.50	1.013 ± 0.03
	13.67 ± 0.50	1.003 ± 0.03
	15.90 ± 0.50	1.000 ± 0.03
2398	1.24 ± 0.50	0.921 ± 0.03
2399	6.37 ± 0.50	1.034 ± 0.03
2400	1.69 ± 0.50	0.979 ± 0.03
	5.16 ± 0.50	1.027 ± 0.03
	6.69 ± 0.50	1.027 ± 0.03
2705	0.82 ± 0.15	0.858 ± 0.03
	1.61 ± 0.15	0.882 ± 0.03
	2.19 ± 0.15	1.009 ± 0.03
	2.50 ± 0.15	0.969 ± 0.03
	2.93 ± 0.15	1.020 ± 0.03
	3.06 ± 0.15	1.002 ± 0.03
2706	0.80 ± 0.15	0.789 ± 0.03
	1.05 ± 0.15	0.820 ± 0.03
	1.20 ± 0.15	0.818 ± 0.03
	1.22 ± 0.15	0.927 ± 0.03
	1.23 ± 0.15	0.864 ± 0.03

*3.18 mm diameter projectile and 0.85 mm thick target.

Table III

Cu-Cu Hole Growth at 7 km/sec*

Shot No.	Time (μsec)	$D_D/D_F \left(\frac{\text{Dia During}}{\text{Dia Final}}\right)$
2393	1.10 ± 0.50	0.713 ± 0.02
	1.74 ± 0.50	0.810 ± 0.02
	2.07 ± 0.50	0.837 ± 0.02
2394	3.42 ± 0.50	0.920 ± 0.02
	4.92 ± 0.50	0.952 ± 0.02
	6.87 ± 0.50	0.968 ± 0.02
	8.30 ± 0.50	0.975 ± 0.02
2396	8.22 ± 0.50	0.979 ± 0.02
	9.33 ± 0.50	0.981 ± 0.02
	14.30 ± 0.50	1.000 ± 0.02
	19.56 ± 0.50	1.000 ± 0.02
2709	0.84 ± 0.15	0.664 ± 0.02
	1.68 ± 0.15	0.784 ± 0.02
	2.50 ± 0.15	0.861 ± 0.02
	3.48 ± 0.15	0.934 ± 0.02
	3.58 ± 0.15	0.922 ± 0.02
2717	0.20 ± 0.15	0.487 ± 0.02
	0.55 ± 0.15	0.625 ± 0.02
	0.99 ± 0.15	0.656 ± 0.02
	5.47 ± 0.15	0.924 ± 0.02

*3.18 mm diameter projectile and 0.85 mm thick target.

Table IV

Cd-Cd Hole Growth at 7 km/sec*

Shot No.	Time (μsec)	$D_D/D_F \left(\frac{\text{Dia During}}{\text{Dia Final}}\right)$
2710	0.55 ± 0.15	0.334 ± 0.02
	1.14 ± 0.15	0.547 ± 0.02
	1.89 ± 0.15	0.641 ± 0.02
	2.86 ± 0.15	0.744 ± 0.02
	3.23 ± 0.15	0.769 ± 0.02
2716	0.96 ± 0.15	0.416 ± 0.02
	1.23 ± 0.15	0.534 ± 0.02
	5.55 ± 0.15	0.903 ± 0.02
	5.81 ± 0.15	0.905 ± 0.02
	9.00 ± 0.15	0.945 ± 0.02

*3.18 mm diameter projectile and 0.85 mm thick target.

Table V

Al-Al Hole Growth at 7 km/sec*

Shot No.	Time (μsec)	$D_D/D_F \left(\frac{\text{Dia During}}{\text{Dia Final}}\right)$
2714	0.92 ± 0.15	0.477 ± 0.02
	1.69 ± 0.15	0.738 ± 0.02
	2.36 ± 0.15	0.878 ± 0.02
	2.79 ± 0.15	0.892 ± 0.02
2715	0.88 ± 0.15	0.622 ± 0.02
	1.03 ± 0.15	0.588 ± 0.02
	5.75 ± 0.15	0.965 ± 0.02
	9.00 ± 0.15	1.004 ± 0.02

*6.36 mm diameter projectile and 1.70 mm thick target.

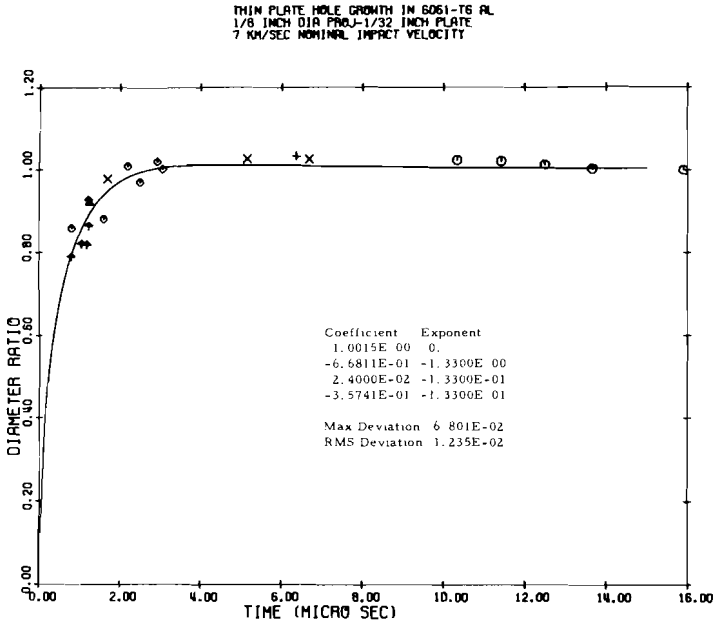

Figure 5. Hole Growth in 6061-T6 Aluminum (3.18 mm Pellets)

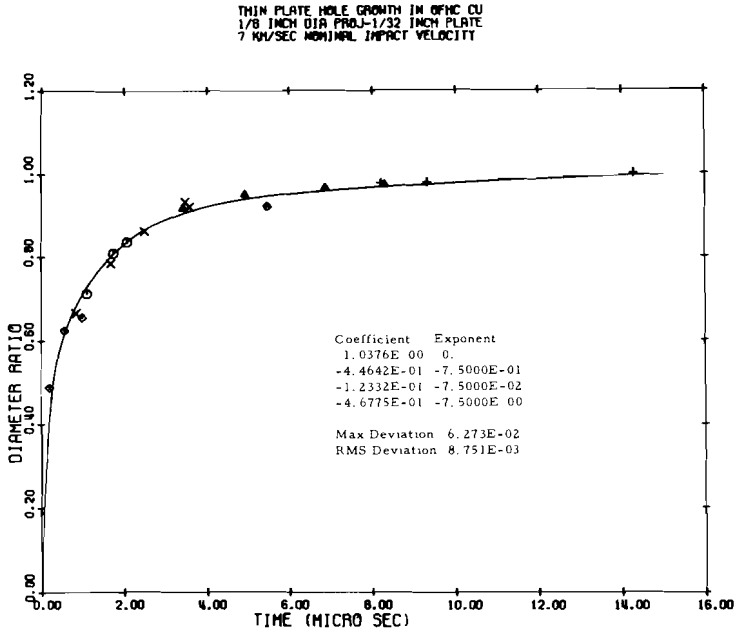

Figure 6. Hole Growth in OFHC Copper (3.18 mm Pellets)

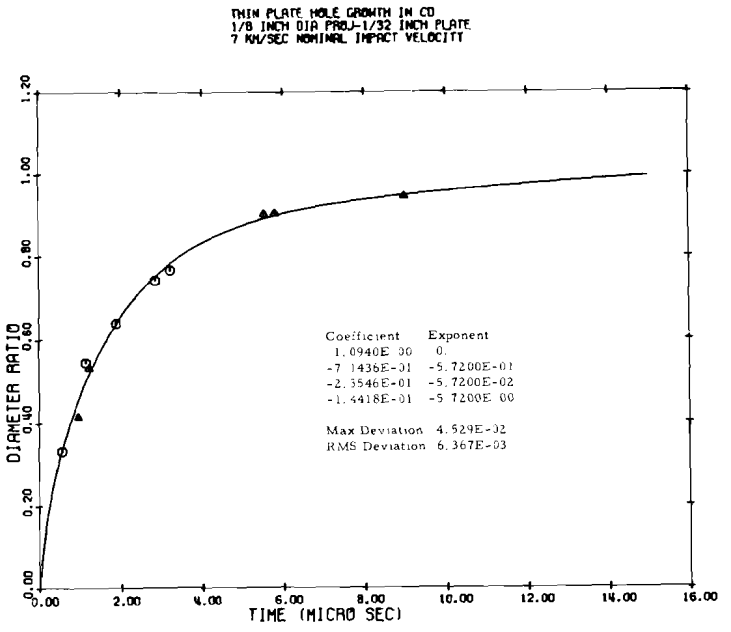

Figure 7. Hole Growth in Cadmium (3.18 mm Pellets)

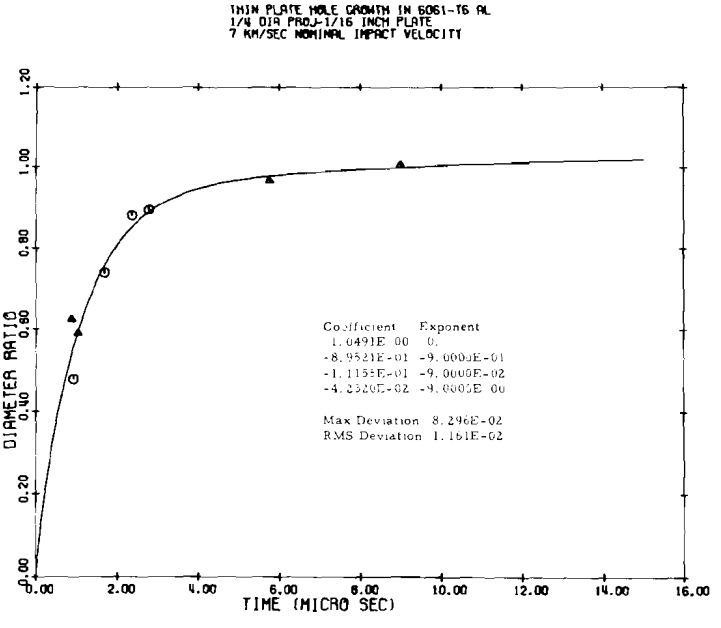

Figure 8. Hole Growth in 6061-T6 Aluminum (6.36 mm Pellets)

where the B_i's are preselected and the A_i's computed by the method of least squares. Each graph includes a listing of the coefficients and exponents describing the associated prony series curve. The maximum and standard deviations of the hole diameter vs. time points from these curves are also presented.

All experimental data was reduced by normalizing hole diameters with respect to final diameters measured from identical radiographs taken after the impact event but before the target setup was disturbed. This method is described more fully in Reference 3. (Figure 9 is a set of dual radiographs for a representative copper impact.) This comparison method not only eliminates the need for a direct quantitative measure of the growing hole's diameter, but also produces a normalized measure of hole size that can be plotted directly[3]. If desired, the actual hole size at any time can be obtained from the hole diameter ratio and the measured final hole size.

The precise times with respect to impact of radiographs taken during the dynamic perforation events were computed from both the electrical gap switches and the optical crystals described earlier. Zero (or reference) time on each shot was based on the Mylar/foil perforation switch for the gap switches and impact flash as observed with an optical fiber. Impact and impact flash were shown to occur within less than 150 nsec for all the material configurations treated in this investigation. A typical oscilloscope record demonstrating this fact is pictured in Figure 10. The upper trace represents impact flash recorded with a photomultiplier tube, and the lower trace, the signal generated by a Mylar/foil perforation switch. Both traces were initiated at the same time and swept at a speed of 2 μsec/cm. Further resolution of any time difference between the two signals was not attempted since greater accuracy was unnecessary. Jitter in the gap switches was found to be greater than 150 nsec, and thus provided sufficient justification for use of optical crystals as the primary means of time determination. With this system, a reasonable bound on the accuracy of any given radiograph time is $-50 < t < 200$ nsec.

The data presented here reinforces and extends the conclusions first proposed in Reference 3. For the three materials treated, hole growth is seen to be a two stage process. The first is one of rapid growth where the hole grows to a large fraction of its final size in a small fraction of the total growth time. The second stage is a longer and slower hole expansion to final size. This two stage mechanism is most pronounced in 6061-T6 aluminum and least evident in cadmium. It is also clearly distinquishable in the scaled up configuration for aluminum. For all materials treated, the hole growth rate was found to be well represented by a four term prony series, one of the terms being a constant. Each set of data can also be approximated by a function of the form:

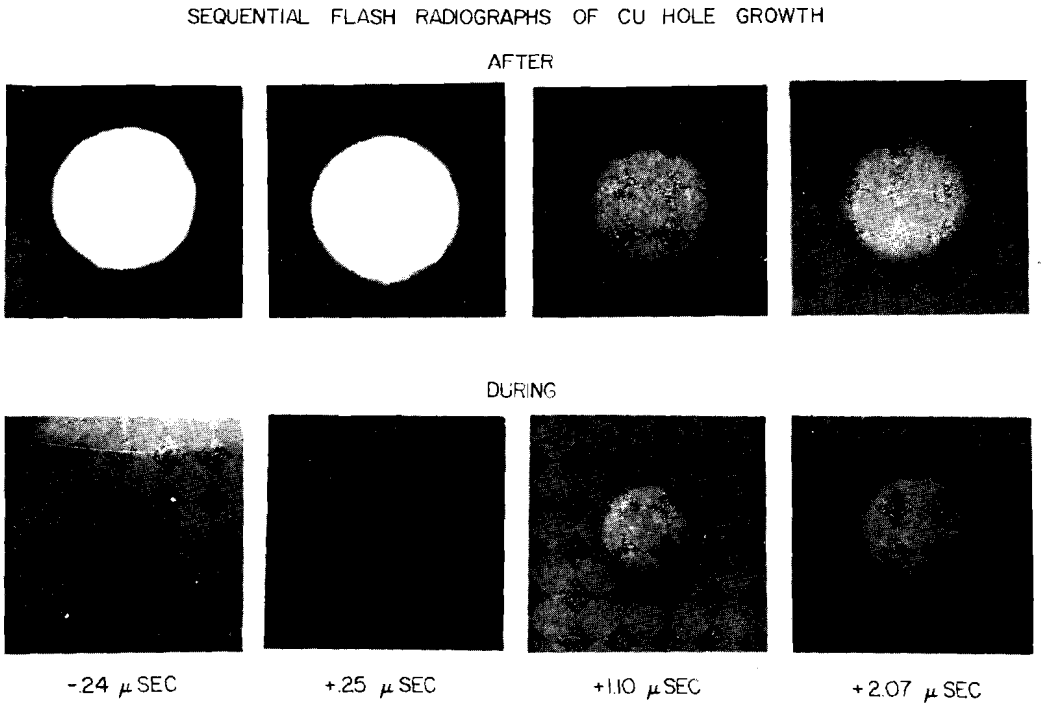

Figure 9. Typical During and Final Radiographs of Hole Growth in Copper

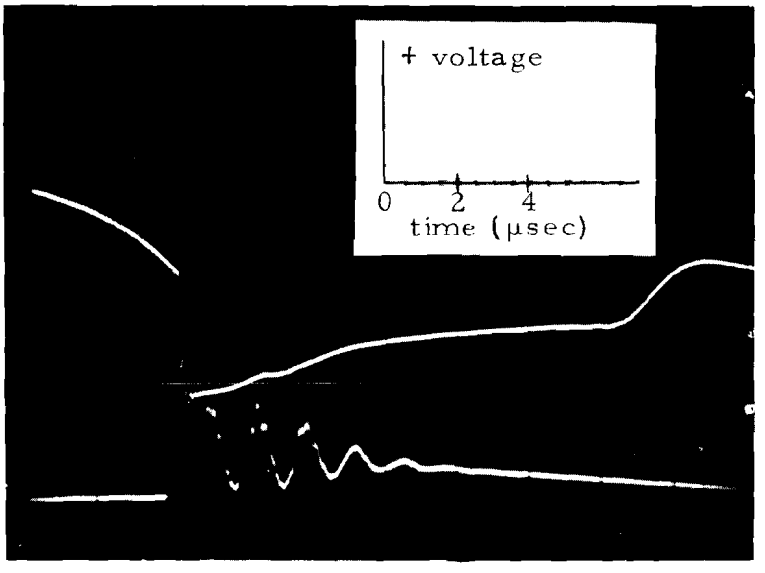

Figure 10. Oscilloscope Record of Impact Flash (Upper) Versus Impact Switch (Lower) at 2 μsec/cm

$$\frac{D_D}{D_F} = 1-e^{kt}$$

D_D = hole diameter at time t

D_F = final hole diameter

k = negative constant

t = time after impact

however, which is indicative of the logrithmic nature of all observed growth rates.

Figures 11 through 13 show the comparison between experimental hole diameter vs. time plots and those predicted by the STEEP code for aluminum, copper, and cadmium, respectively. The experimental curves are the early-time portion of the prony series fits shown without the individual data points. The computer predicted curves are those resulting from the STEEP code and are plotted as dotted lines. The range of prediction is limited because hole growth rates were only a supplementary

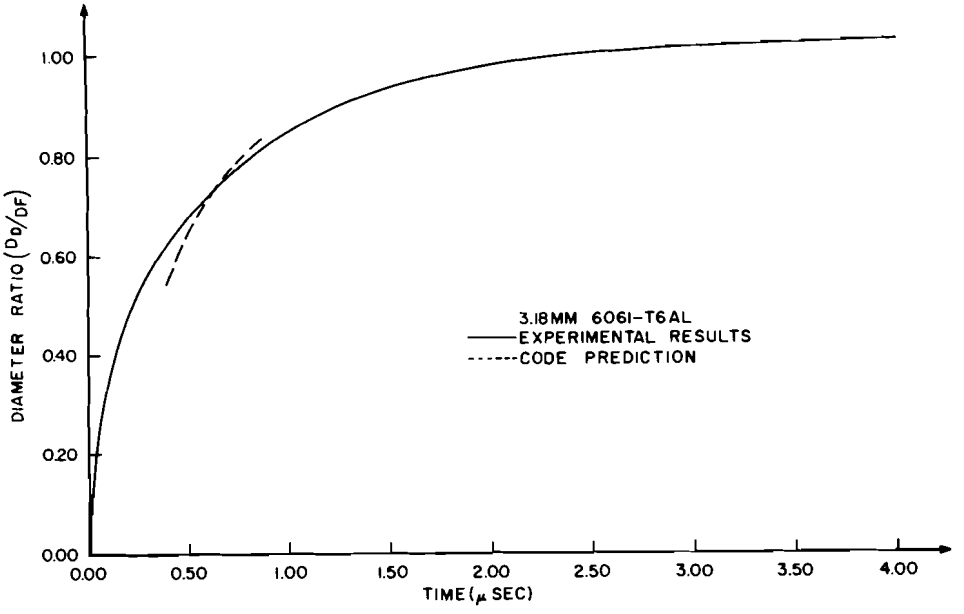

Figure 11. Comparison of Experimental and Predicted Hole Growth for 6061-T6 Aluminum

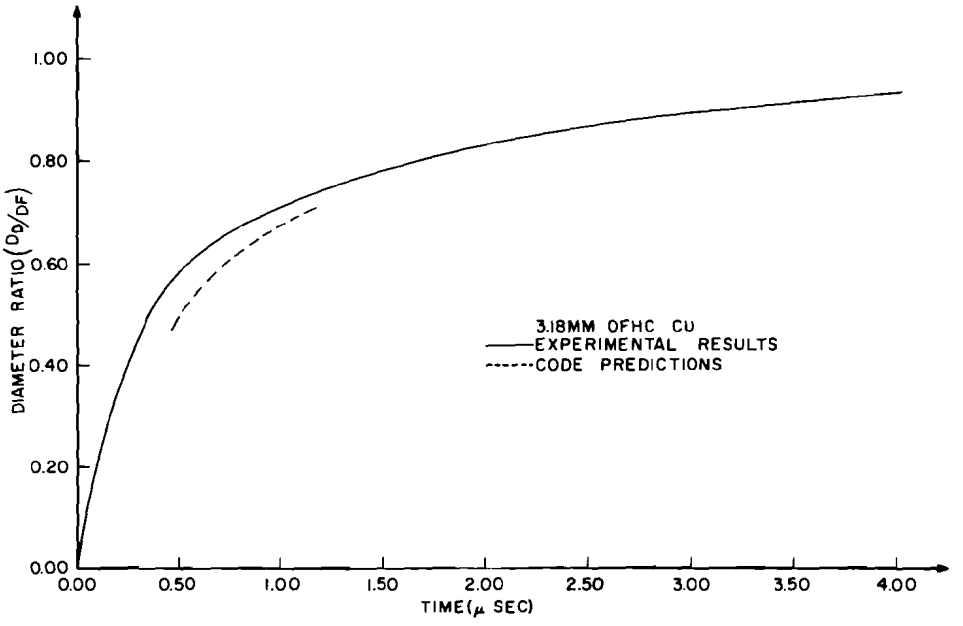

Figure 12. Comparison of Experimental and Predicted Hole Growth for OFHC Copper

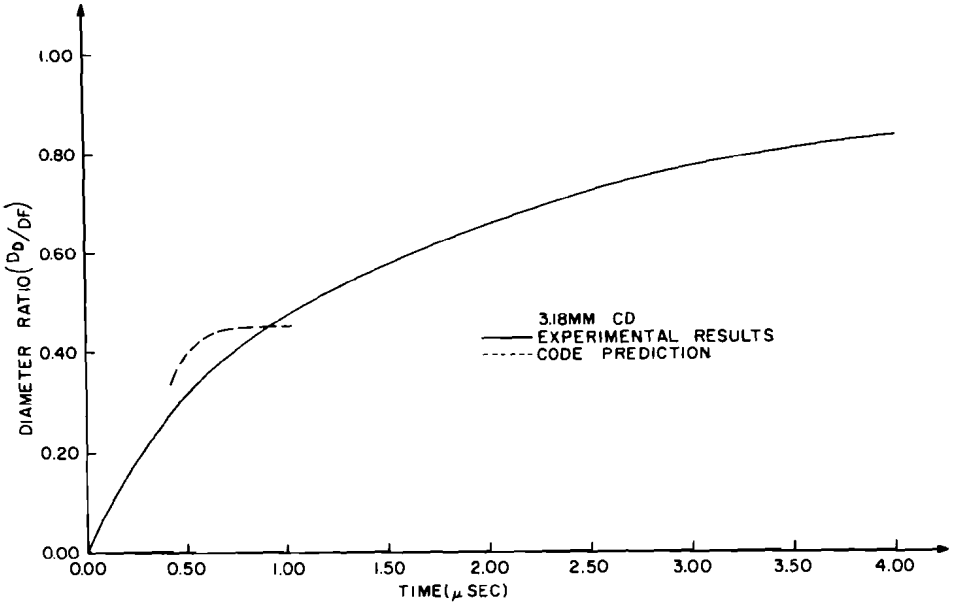

Figure 13. Comparison of Experimental and Predicted Hole Growth for Cadmium

part of the numerical study which was intended to provide comparisons of debris cloud predictions with laboratory experiments. Accordingly, little attempt was made to assure the validity of the hole growth phase of the numerical results.

The numerical calculations were not carried to the point where material flow was arrested and hole size was estimated by application of the dynamic pressure criterion. The largest radius in the target at which the dynamic pressure ($1/2\ \rho \left| \vec{u}^2 \right|$ ρ material density, u particle velocity), equaled the yield stress was taken as the hole radius. Dynamic pressure is the pressure a moving mass would feel if the flow were suddenly stopped. The numerical predictions of hole growth rates, while in error to varying degrees, are not consistent in their disagreement. This fact would appear to define the problem as being associated with the fundamental relationships of material properties to the mechanisms controlling the perforation process and not dependent upon computational techniques. Basic knowledge of the mechanisms controlling impact damage at laboratory achievable velocities must be investigated further in order to define the important fundamental effects of material parameters.

Figure 14 provides a means to examine some aspects of size scaling for thin plate perforation. The prony series curve representing hole growth in the scaled up configuration for aluminum (as shown in Figure 8) is

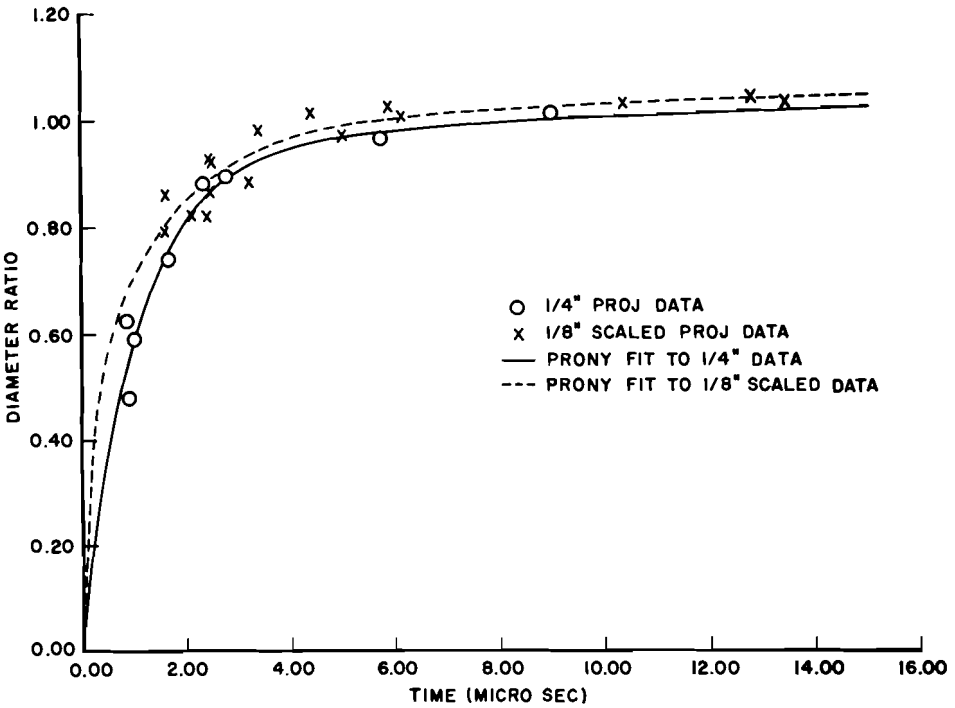

Figure 14. Comparison of Actual and Size Scaled Experimental Hole Growth Data in 6061-T6 Aluminum

directly plotted as a solid line with individual data points appearing as circles. A second prony series curve representing the standard configuration for aluminum, but fit to twice the experimentally recorded times is plotted on the same graph as a dotted line. The data points for this plot are shown as crosses. Since the normalized hole diameter term is size independent, the two curves should theoretically be the same if size scaling occurs for the thin plate perforation event. Considering the scatter of the data points the two curves are consistant. There is a possibility that the first stage of hole growth does not directly scale in the two cases. Unfortunately, there are insufficient early time data points for the standard aluminum configuration to justify conclusive arguments at this time. Complete resolution will require considerable hole growth data points for this scale of impact in the zero to 500 nsec real time range. This is more difficult than at first apparent since the mass of the projectile occupies the newly formed hole during much of this time. AFML is currently developing the required improvements in radiograph techniques to carry out the desired experiments.

III. FINAL HOLE SIZE IN THIN PLATES

Investigators of hypervelocity impacts into thin plates have traditionally tried to formulate equations capable of predicting the final hole size generated in the thin plate. Various visco-plastic and hydrodynamic models have been employed to describe hole generation and semi-empirical relationships have been made to predict hole size for specific cases.

One of the earlier equations was formulated by Rolsten, et al[8]. Using an impact model in which material was displaced by radial flow from an annular ring in the plate about the impacting pellet the following equation was derived for thin plate perforation caused by normal impact with a cylinder:

$$\frac{D_{max}}{do} = \left[2 + \left(\frac{\rho_t}{\rho_p} \right)^{1/2} \right]^{1/2} \qquad (1)$$

(where D = hole diameter, ρ_t = target density, ρ_p = pellet density, and do is greater than the original pellet diameter, d, by a percentage (R) dependent upon a term called the acceleration velocity (I). R = 0.00256 I - 5.8) Empirical correlation with a limited number of experimental data points lead to the proposal that $D_F = 0.9\ D_{max}$. Hole "rebound" was identified as the basis for this modification. Even with the use of this modification however, predictions poorly match other experimental results. Hole "rebound" has since been investigated and found to have a negligible effect on final hole size[3].

Considerable efforts have since been made to derive hole diameter equations capable of fitting specific blocks of experimental data. One such equation, which was generated to describe data resulting from 3.2 mm Al spheres impacting 2024-T3 Al plates, was proposed by Maiden and McMillan[9]*.

$$\frac{D_F}{d} = 2.4\ \frac{V}{C} \left(\frac{t_s}{d} \right)^{2/3} + 0.9 \qquad (2)$$

(where t_s = plate thickness, V = impact velocity, C = material sonic velocity). It relates final hole size to impact velocity and plate thickness. An equation of a similar form has been developed by Nysmith and Denardo[10]** to fit data generated by both 3.2 mm pyrex and aluminum pellets impacting 2024-T3 Al plates.

---

* General Motors Defense Research Laboratory (GMDRL).

** NASA, Ames Research Center (NASA Ames).

$$\frac{D_F}{d} = 0.88\,\rho_p^{1/2}\left(\frac{t_s}{d}\right)^{0.45} V^{1/2} \qquad (3)$$

This equation was made subject to the restriction that front and rear surface effects are negligible thus requiring relatively thin sheets and high impact velocities. These conditions do not place undue restrictions upon practical applications for their equation. A final equation which deserves special attention due to its use by NASA Manned Spacecraft Center[11] was developed by McHugh* using multiple regression analysis upon a large block of experimental data[12].

$$\frac{D_F}{d} = 0.658\left(\frac{t_s}{d}\right)^{0.14} (\varepsilon)^{0.22} V \exp\left[0.63\left(\frac{t_s}{d}\right)^{0.43}\right] \qquad (4)$$

In this case ε is the ultimate room temperature tensile strain (measured in percent) of the impacting pellet and target sheet material.

The formulations of a hole diameter equation as seen usually include such parameters as impact velocity, plate thickness, and pellet size, plus pellet and target material terms such as density, strength and shock properties. It might be noted that equations 2-4 are of essentially the same form (see Table VI) containing a constant, a velocity term to some power, and a plate thickness-pellet diameter ratio (t_s/d) to some power. In each case however, a different term related to the materials subjected to impact is used. Since the impact cases considered in the AFML study involve materials with widely different mechanical properties, shock properties, and densities, the usefulness of the materials factors used in the three materials may be partially evaluated. The limited range of experimental data however, makes the correlation and refinement of equations such as those mentioned above difficult.

The Air Force Materials Laboratory has accumulated a block of hole diameter data from hypervelocity impacts of thin plates during various impact studies. Appendix I contains the computer catalog of this data containing some 400 data points. The majority of the shots reported in this Appendix employed 3.2 mm 2017 Al spheres impacting several thicknesses of 6061-T6 Al bumpers.

Using the method of least squares, these hole diameters were related to pellet velocity, momentum, and energy for each bumper thickness. The standard deviations of the points about each of these fits are equivalent as shown in Table VII. This result indicates that, for this

---

* North American Rockwell Corporation, Space Division (NARC).

Table VI

Comparison of Hole Diameter Equation Terms

Equation	Velocity Term	Plate Thickness Pellet Diameter Ratio	Materials Term
2	V	$\left(\frac{t_s}{d}\right)^{2/3}$	$\frac{1}{C}$ (1)
3	$V^{1/2}$	$\left(\frac{t_s}{d}\right)^{0.45}$	$\rho_p^{1/2}$ (2)
4	$V_{exp}\left[0.63\left(\frac{t_s}{d}\right)^{0.43}\right]$	$\left(\frac{t_s}{d}\right)^{0.14}$	$\varepsilon^{0.22}$ (3)

1. C = sonic velocity
2. ρ_p = pellet density
3. ε = ultimate elongation

Table VII

Standard Deviation (Expressed in Percent of Median Hole Diameter) of Least Square Equations Relating Hole Diameter to Pellet Velocity, Momentum, and Kinetic Energy for Each Plate Thickness.

Al-Al Impact Case
0.32 cm dia Al Sphere (6.75 km/sec)

Plate Thickness (mm)	No. Data Points	$\sigma(v)$	$\sigma(mv)$	$\sigma(1/2\ mv^2)$
0.406	6	0.49%	0.51%	0.50%
0.635	3	0.08%	0.10%	0.10%
0.787	25	1.14%	1.14%	1.33%
0.813	15	1.24%	1.24%	1.63%
0.838	80	2.36%	2.31%	2.36%
1.600	15	0.77%	0.73%	1.12%
2.540	5	2.05%	2.02%	2.03%
2.565	7	0.49%	0.51%	0.41%
3.175	3	0.47%	0.43%	0.48%

velocity range (6-7.5 km/sec), hole diameter is an insensitive function of velocity and that the small deviation in the mass of the pellets was not significant. It was noted however, that the slope of the hole diameter vs. velocity plots increases with increasing bumper thickness for several cases of similar material impacts (see Figure 15). Target plate thickness has a strong influence upon hole diameter. It may also be noted from Figure 15 that as the bumper thickness tends toward zero the velocity dependence of hole diameter vanishes. This result has been confirmed experimentally over wide velocity ranges. Once target perforation velocity is achieved, hole size in very thin plates is nearly the same size as the pellet. It is also obvious that there is a critical target thickness for a particular impact velocity where no perforation occurs, and hence the hole diameter is zero. The hole formation process becomes a combination of front surface cratering and rear surface spallation rather than behaving like a thin plate well before ballistic limit conditions are reached, however. These facts are depicted in Figure 16 which shows hole diameter vs. plate thickness both normalized to the pellet diameter for Al-Al impacts at 7 km/sec. Note that at very small t_s/d ratios the hole diameter equals the particle diameter and at some critical t_s/d ratio, in this case approximately 3.5, a hole is not formed. If the possibly questionable assumption of linear size scaling is made, then the relationship seen in Figure 17 can be developed. This figure shows hole diameter vs. pellet diameter both normalized to plate thickness. Such a curve is useful in determining

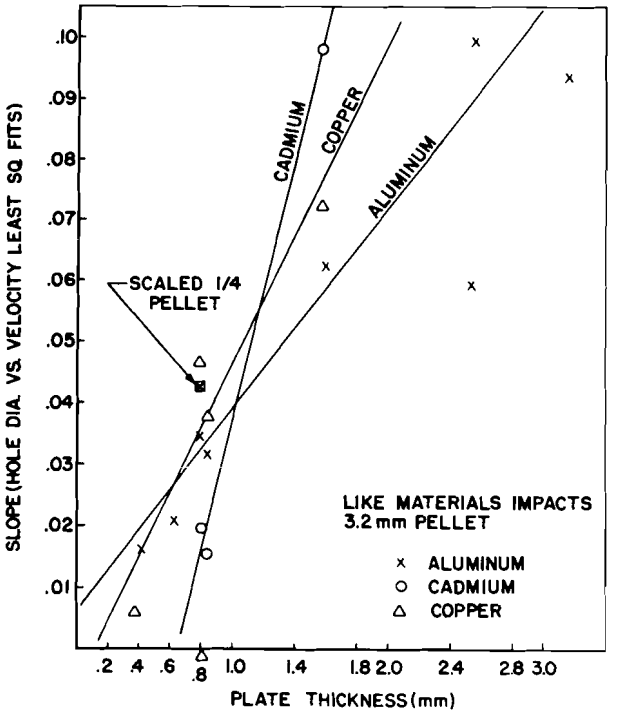

Figure 15. Slope of Hole Diameter vs. Velocity Equations vs. Plate Thickness

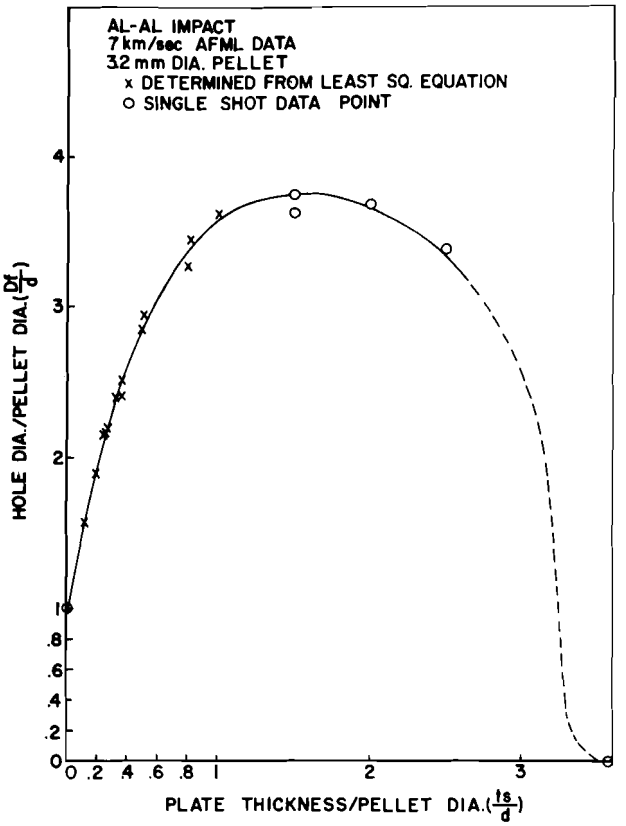

Figure 16. Hole Diameter vs. Plate Thickness Normalized to Pellet Diameter (Al-Al Impact at 7 km/sec)

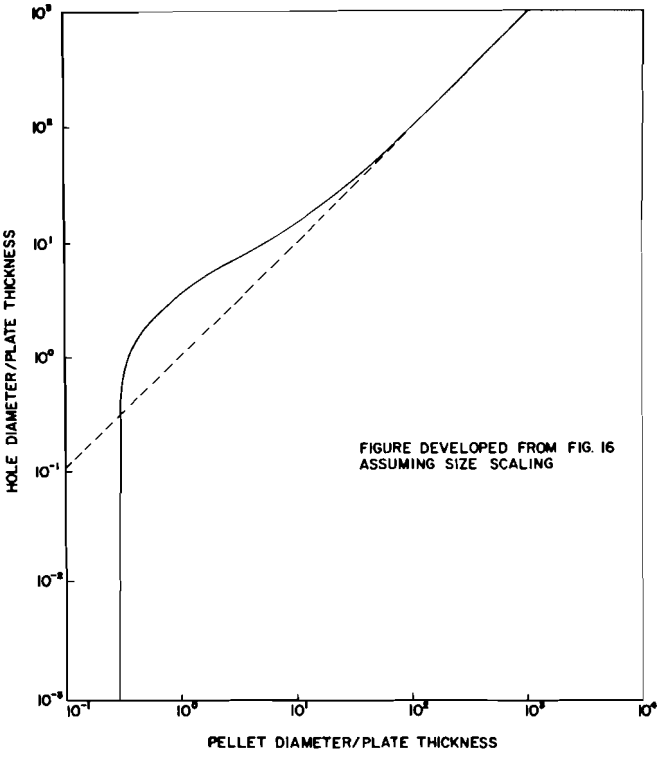

Figure 17. Hole Diameter vs. Pellet Diameter Normalized to Plate Thickness (Al-Al Impact at 7 km/sec)

the size of an unknown particle responsible for a given hole in a thin witness plate. Note that when the final hole-plate thickness ratio (D_F/t_s) is above 10^2 there is a one to one correspondence between hole diameter and pellet diameter. When this ratio decreases below one the technique is not useful in determining pellet size. The limitation to this technique then is how thin one can make a witness plate if the size distribution of the expected particles is unknown.

The AFML data relating hole diameter to pellet velocity and plate thickness is compared to the predictions of the equations from GMDRL (Eq. 2), NASA Ames (Eq. 3), and NARC (Eq. 4) in Figures 18-20. Like material impacts involving aluminum, copper, and cadmium are considered. In all cases the pellets were 3.2 mm spheres while the thin plates were 6061-T6 Al, OFHC Cu, and commercially pure cadmium. Figure A for each material presents hole diameter vs. impact velocity for several bumper thicknesses. The AFML data is represented by a least squares line fit to the data for a particular bumper thickness. The lines representing the predictions of Equations 2-4 for a particular bumper thickness were generated using the values for ρ_p, ε, and C shown in Table VIII. Although each of the equations uses a different power velocity term, it may be noted that over the velocity range of the graphs they all appear as essentially straight lines. Figure B for each material relates hole diameter to plate thickness for an impact velocity of 7.0 km/sec. The AFML experimental curves were generated by using the least squares equation fitting the data for each bumper thickness with respect to velocity and selecting the 7.0 km/sec intercept. In general the predictions of each equation matches the general form of the experimentally observed results although various errors do appear.

The GMDRL Equation (2), although developed for impacts onto 2024-T3 Al, fails to accurately predict results with increasing error as t_s/d increases. Similar low predictions of hole diameter result for the copper case while for the cadmium case the predictions tend to be high.

The NASA Ames Equation (3) which employs a material density term and was also developed for aluminum impacts, shows good correlation with the AFML aluminum data except at small t_s/d ratios. Due to the nature of the equation as $t_s \longrightarrow 0$, D_F must also approach 0. For the copper and cadmium cases however, the predictions are consistantly high.

The NARC Equation (4) employing a maximum elongation term to describe materials response predicts experimental aluminum data quite accurately except at the higher t_s/d ratios. Underestimations of hole diameters result for the other two materials. It is interesting that GMDRL and NARC agree for copper while NASA and GMDRL agree for cadmium and all three essentially agree for aluminum. These disparities can likely be traced to the fairly small effect a number of parameters have

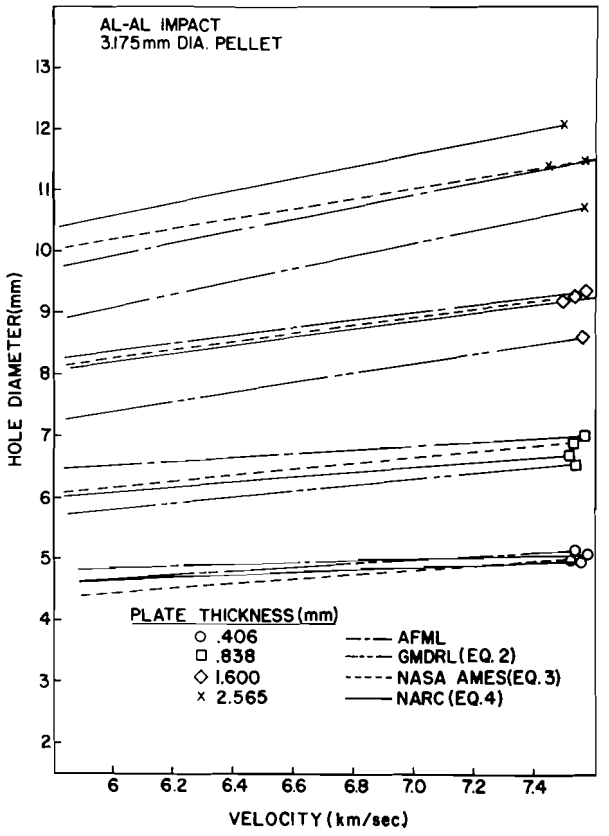

Figure 18a. Hole Diameter vs. Velocity (Al-Al)

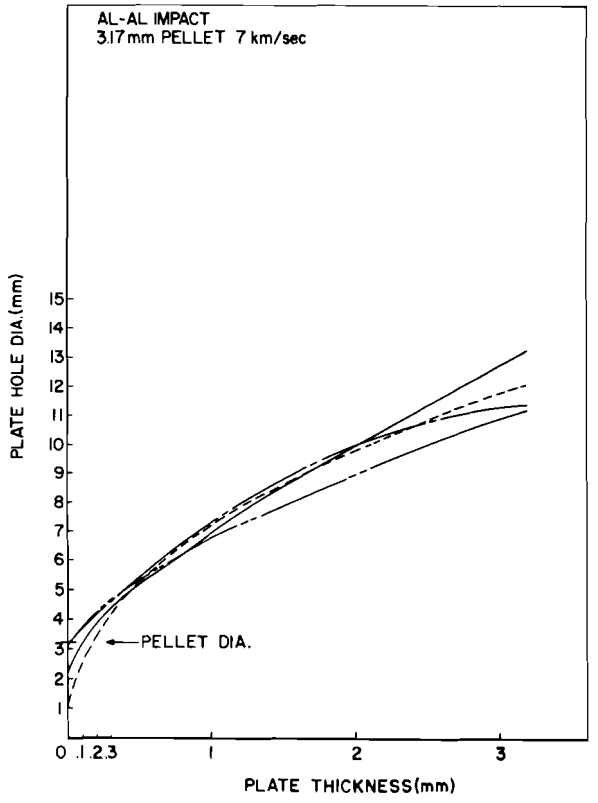

Figure 18b. Hole Diameter vs. Plate Thickness (Al-Al)

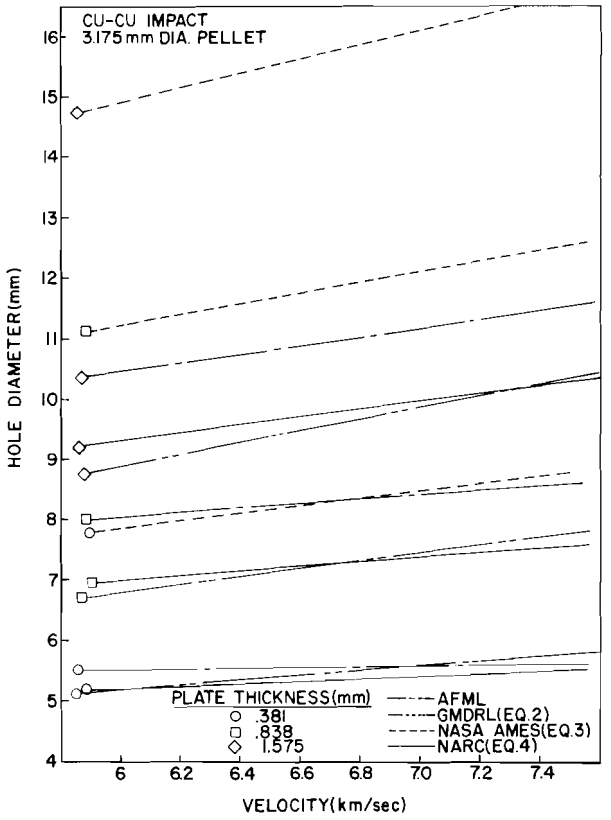

Figure 19a. Hole Diameter vs. Velocity (Cu-Cu)

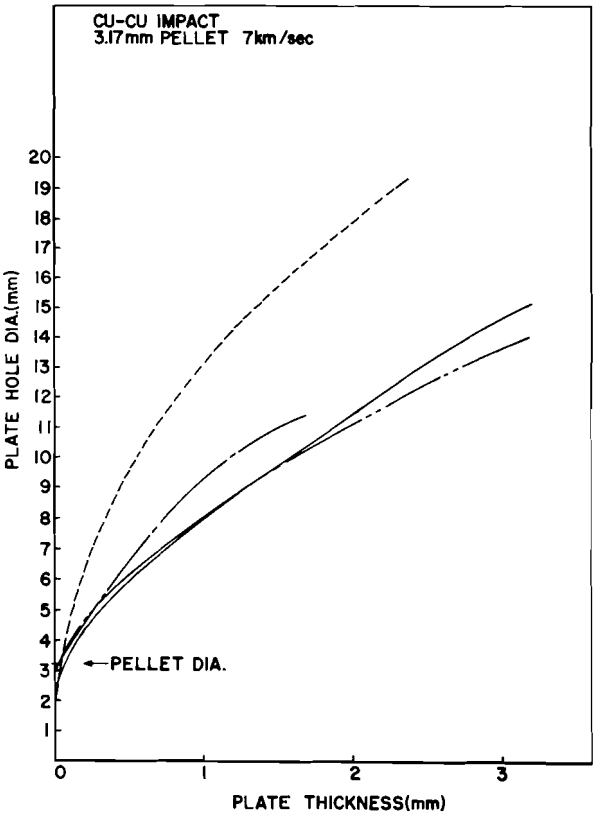

Figure 19b. Hole Diameter vs. Plate Thickness (Cu-Cu)

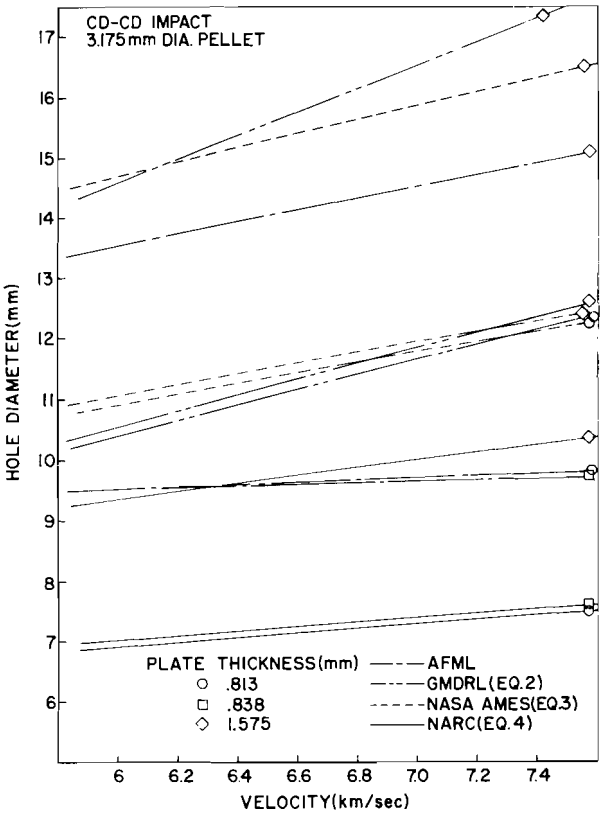

Figure 20a. Hole Diameter vs. Velocity (Cd-Cd)

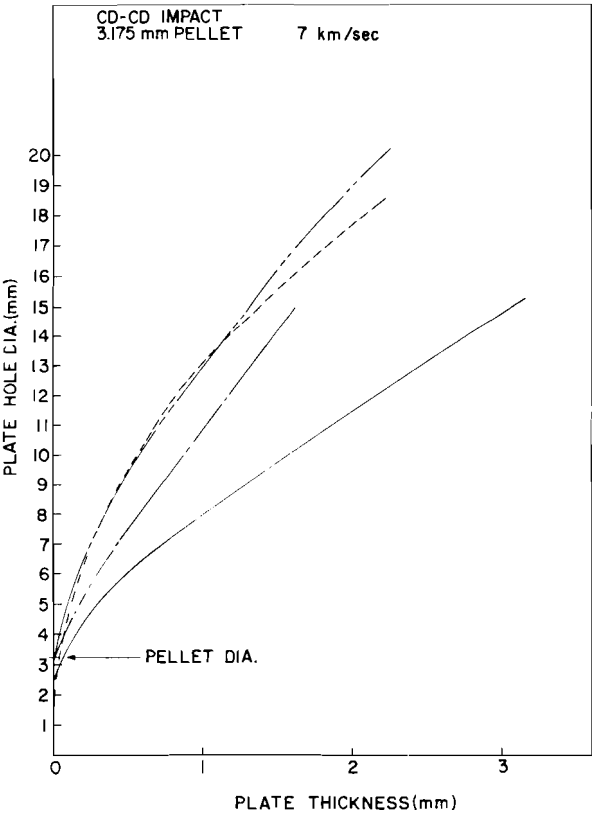

Figure 20b. Hole Diameter vs. Plate Thickness (Cd-Cd)

Table VIII

Material Parameters* Used for Equations 2-4

	Al	Cu	Cd
C (mm/μsec)	6.36	4.77	2.44
ρ_p (gm/cm^3)	2.70	8.90	8.64
ε (percent strain)	17%	31%	32%

* Measured for particular AFML materials impacted.

upon the final hole size. In order to isolate the various effects of all these parameters one needs a very wide variety of data over a wide velocity range probably covering many thousands of firings.

IV. CONCLUSIONS

By combining the information presented in this study and in References 3 and 6, it is possible to develop a reasonable qualitative model of thin plate impact. A brief discussion of the related information leading to the proposal of this model will be presented here in the form of a review of pertinent AFML experimental results pertaining to thin plate hole growth. The energetic debris comprising the central portion of all observed debris clouds behind impacted plates was shown to contain most of the original pellet material[3, 6]. This material was found to originate from areas on impacted plates significantly smaller than the final holes in these plates[6]. The areas of debris origin were circular, centered about the initial impact points and were about the same diameter as the original pellet (Figure 21). The experimental results pertaining to debris origin are in good agreement with the qualitative predictions of the STEEP impact code[5]. Quantitative determination of the velocity profiles across debris clouds, and the exact position in space of this debris at some given time after impact, are also available[3]. This data permits extrapolation of debris positions back to impact time. Comparisons of this departure sequence with the hole growth vs. time curves presented in this study indicate that the highly energetic central debris cone (containing most of the pellet material) departs the impacted plate during the first (or rapid) stage of hole growth. The logrithmic form of all observed hole growth rates, particularly in the second (or slower) stage of growth, indicate the possible involvement of the dilatational wave generated by impact as a controlling factor in thin plate hole growth. The decay rate of such a wave with radial expansion would be compatible with the observed hole growth rate, especially in the slower second stage. Strain gage measurements of these waves are presented in Reference 3. As noted earlier, the hole size approaches the pellet diameter as the ratio of plate thickness-pellet diameter approaches zero. This supports the idea that the dilatational wave produces the second stage of hole growth. For very thin targets this wave would be rapidly decayed by boundary reflections and thus second stage hole growth would be minimal.

With the preceding observations as a basis, then, the following qualitative description of a thin plate impact is proposed. The pellet contacts the plate; and although compressive deformation and tensile fracture commence, the pellet mass does not significantly disperse as it penetrates the plate. The pellet material does not disperse because the pellet velocity initially exceeds or is of the same order as the velocities of all shock waves generated in the pellet and plate material. When the pellet mass and displaced plate mass emerge from the rear surface of the plate, they disperse in a generally downrange direction. The hole growth rate to this point for a spherical pellet impacting a plate with a thickness less than one-half the pellet diameter has essentially been identical to the closure velocity perpendicular

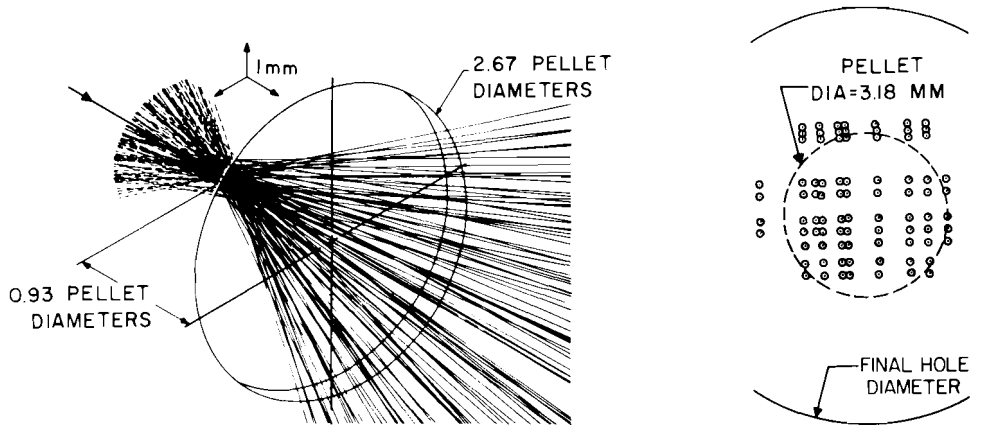

Figure 21. Typical Debris Origin Extrapolation Data for 7 km/sec Thin Plate Impacts

to trajectory. For thicker plates this velocity would begin to vary since the closure velocity would go to zero before the leading projectile edge had reached the plate rear surface. For the nominal conditions of the impact experiments discussed herein, then, the total time of correspondence between hole growth and closure velocity would be equal to the time in which the pellet travels its radius or 228 nsec. This is in general agreement with the STEEP code predictions for material displacement as a function of time presented in Reference 5.

Beyond the point where the pellet and hole diameters are the same, the shock propagates radially outward through the plate. It simultaneously undergoes interaction with reflections from free surfaces. A transition zone exists during this period where the hole growth rate is controlled by front and rear surface spall in combination with the outward moving shock. At some later point the magnitude of the outward moving pulse is attenuated sufficiently by interaction with boundary reflections, and material damping due to inelastic, irreversible particle interactions, that surface spall no longer occurs. The second stage of hole growth begins here and extends to the final hole size. It is controlled by the decay rate of the outward propagating wave which is logrithmic in nature. The hole ceases to grow when this wave becomes completely elastic, with the possible exception of a 0 to 3 percent elastic rebound (indications of this were observed in the experimental curves for 6061-T6 aluminum). The attenuation of this second stage growth process is thus controlled by the shock and material properties of the target. The slope of a line such as seen in Figure 15 which relates hole diameter to target thickness and is an indication of this second stage process may possibly be used to determine the nature of the combined effects of shock and materials properties on the arresting of hole growth.

It must be stressed that this model is meant to be qualitative only and is proposed solely as an explanation capable of accounting for the observed effects. The authors do intend, however, to point out the fact that the experimental evidence presented here and in related AFML studies does indicate that hole growth in hypervelocity impacted thin plates is not a simple single stage process. It is hoped that the qualitative discussions and quantitative data contained herein will provide useful assistance in better understanding this important aspect of hypervelocity interactions.

REFERENCES

1. Whipple, F. L., "The Meteoric Risk to Space Vehicles", Vistas in Astronautics, Vol. II, New York: Pergamon Press, 1958.

2. Swift, H. F., J. M. Carson, and A. K. Hopkins, Ballistic Limits of 6061-T6 Aluminum Bumper Systems, AFML-TR-67-324, Wright-Patterson AFB, Ohio: AFML, October 1967.

3. Turpin, W. C., Hypervelocity Perforation Mechanics of Thin Metal Plates, AFML-TR-69-203, Wright-Patterson AFB, Ohio: AFML, July 1969.

4. Tillotson, J. H., A Theoretical and Experimental Correlation of Hypervelocity Impact on Layered Targets, EG&G Technical Report 5-425-R, May 1968.

5. Rosenblatt, M., K. N. Kreyenhagen, and W. D. Romine, Analytical Study of Debris Clouds Formed by Hypervelocity Impacts of Thin Plates, AFML-TR-68-266, Wright-Patterson AFB, Ohio: AFML, December 1968.

6. Swift, H. F., D. D. Preonas, W. C. Turpin, and J. H. Cunningham, "Characterization of Debris Clouds Behind Impacted Meteoroid Bumper Plates", AIAA Paper No. 69-380, Proceedings, AIAA Hypervelocity Impact Conference, Cincinnati, Ohio: AIAA, 1969.

7. Swift, H. F. and E. A. Strader, "Flash X-ray Actuated Trigger Switch", The Review of Scientific Instruments, Vol. 39, No. 5, May 1968.

8. Rolsten, R. F., J. N. Wellnitz, and H. H. Hunt, "An Example of Hole Diameter in Thin Plates Due to Hypervelocity Impact", Journal of Applied Physics, Vol. 35, No. 3, March 1964.

9. Personal communication with Mr. A. R. McMillan of General Motors Defense Research Laboratory, Warren, Michigan.

10. Nysmith, C. R. and B. P. Denardo, Experimental Investigation of the Momentum Transfer Associated With Impact Into Thin Aluminum Targets, NASA TN-D5492, October 1969.

11. Personal communication with Mr. B. G. Cour-Palais, NASA Manned Spacecraft Center, Houston, Texas.

12. McHugh, A. H., Evaluation of Hypervelocity Impact Damage to a Thin Sheet by Multiple Regression Analysis, NAA/S&ID Report STR 152, June 1966.

APPENDIX

COMPILATION OF HOLE-SIZE DATA

FOR HYPERVELOCITY IMPACTS OF THIN PLATES

The data listed in this appendix was generated on the AFML 40 mm-30 cal. light-gas gun. The impacting pellets were enclosed in sabots during the launch process so that their masses and shapes were not affected by the launch process. The pellet trajectory was evacuated sufficiently to insure neither significant deceleration nor ablation during flight. Pellet velocities were measured to within $\pm$ 0.25% using a two station streak system. Pellet mass was determined to within $\pm$ 0.2% by weighing prior to launch. Pellet condition after launch was monitored photographically and in no case was pellet deformation observed.

The diameters of the final holes in the targets were measured to within $\pm$ 0.05 mm with vernier calipers. In those cases where the holes were found to be noncircular, such as was the case for cadmium and paraffin plates, several measurements of the hole were made and the average recorded.

PROJECTILE						BUMPER		ROUND NO.
MATERIAL	SIZE (CM)	MASS (MG)	VELOCITY (KM/SEC)	MOMENTUM (KGM/SEC)	ENERGY (JOULES)	MATERIAL	THICKNESS (MM)	HOLE DIA. (CM)	
ALUMINUM	0.157	5.90	7.010	0.0414	145.	CARBON	0.406	0.339	2699
	0.159	6.00	7.047	0.0423	149.	ALUMINUM	0.381	0.333	2185
		5.98	6.858	0.0410	141.		0.813	1.189	2129
		6.01	6.858	0.0412	141.		0.813	1.168	2127
		5.94	6.839	0.0406	139.	TITANIUM	0.432	0.335	2179
		5.96	6.969	0.0415	145.		0.432	0.335	2167
	0.239	19.90	6.898	0.1373	473.	COPPER	0.406	0.495	2191
		19.98	7.276	0.1454	529.		0.406	0.500	2184
	0.317	45.72	6.103	0.2790	851.	PARAFFIN	2.540	1.708	2320
		46.04	6.291	0.2896	911.		2.540	1.890	2310
		45.88	6.383	0.2929	935.		2.540	1.638	2319
		46.12	6.421	0.2961	951.		2.540	1.840	2311
		45.88	7.297	0.3348	1221.		3.175	1.990	2328
		45.73	6.248	0.2857	893.		4.750	2.410	2332
		45.72	7.145	0.3266	1167.		4.750	2.380	2334
		45.68	7.184	0.3282	1179.		4.750	2.400	2329
		45.90	6.200	0.2846	882.	POLYETHYLENE	2.362	1.048	2308
		45.76	6.373	0.2916	929.		2.362	1.050	2292
		45.82	6.810	0.3120	1062.		2.362	1.100	2304
		47.40	7.074	0.3353	1186.		2.362	1.120	2273
		48.00	7.041	0.3380	1190.		2.362	1.105	2278
		46.00	6.366	0.2928	932.	MG-LI ALLOY	1.575	0.880	2294
		46.20	6.434	0.2973	956.		1.575	0.905	2312
		45.82	6.512	0.2984	971.		1.575	0.870	2296
		45.96	6.556	0.3013	988.		1.575	0.895	2300
		45.80	6.607	0.3026	1000.		1.575	0.893	2306
		45.66	6.798	0.3104	1055.		1.575	0.898	2298
		45.78	6.840	0.3131	1071.		1.575	0.908	2297
		47.80	6.809	0.3255	1108.		1.600	0.905	2276
		47.80	7.017	0.3354	1177.		1.600	0.925	2275

PROJECTILE						BUMPER			
MATERIAL	SIZE (CM)	MASS (MG)	VELOCITY (KM/SEC)	MOMENTUM (KGM/SEC)	ENERGY (JOULES)	MATERIAL	THICKNESS (MM)	HOLE DIA. (CM)	ROUND NO.
ALUMINUM	0.317	45.70	6.590	0.3012	992.	MAGNESIUM	0.686	0.640	2451
		45.58	6.895	0.3143	1083.		0.686	0.665	2452
		45.84	6.901	0.3163	1091.		0.686	0.672	2453
		45.74	7.145	0.3268	1167.		1.041	0.805	2416
		45.78	6.959	0.3186	1108.		1.270	0.848	2368
		45.92	7.081	0.3251	1151.		1.270	0.875	2369
		45.86	7.361	0.3376	1242.		1.270	0.933	2366
		45.79	6.879	0.3150	1084.		3.175	1.180	2443
		45.80	7.010	0.3211	1125.		3.175	1.225	2444
		45.78	6.834	0.3128	1069.	TEFLON	0.508	0.590	2449
		45.80	6.849	0.3137	1074.		0.508	0.590	2448
		45.92	6.876	0.3158	1086.		0.508	0.590	2447
		48.40	6.817	0.3300	1125.		0.991	0.835	2274
		48.00	7.109	0.3412	1213.		0.991	0.860	2272
		45.64	6.797	0.3102	1054.		2.362	1.243	2446
		45.85	6.895	0.3161	1090.		2.362	1.256	2490
		45.72	6.919	0.3163	1094.		2.362	1.275	2491
		45.70	6.951	0.3177	1104.		2.362	1.250	2492
		45.84	6.943	0.3183	1105.		2.362	1.205	2454
		45.70	6.968	0.3184	1109.		2.362	1.205	2445
		45.90	7.013	0.3219	1129.		2.362	1.270	2450
		45.99	7.059	0.3247	1146.		2.362	1.259	2458
		45.91	6.820	0.3131	1068.	ALUMINUM	0.025	0.322	2159
		45.76	6.157	0.2817	867.		0.406	0.485	2089
		45.74	6.601	0.3019	996.		0.406	0.497	2101
		45.74	6.853	0.3134	1074.		0.406	0.495	2091
		45.89	7.150	0.3281	1173.		0.406	0.500	2094
		45.94	7.224	0.3319	1199.		0.406	0.503	2090
		45.80	7.316	0.3351	1226.		0.406	0.507	2192
		45.68	7.111	0.3248	1155.		0.635	0.604	2376
		45.76	7.221	0.3304	1193.		0.635	0.607	2405

PROJECTILE						BUMPER		ROUND NO.
MATERIAL	SIZE (CM)	MASS (MG)	VELOCITY (KM/SEC)	MOMEMTUM (KGM/SEC)	ENERGY (JOULES)	MATERIAL	THICKNESS (MM)	HOLE DIA. (CM)	
ALUMINUM	0.317	45.90	7.266	0.3335	1212.	ALUMINUM	0.635	0.607	2404
		45.20	4.700	0.2124	499.		0.787	0.600	2742
		45.10	4.724	0.2131	503.		0.787	0.604	2741
		45.73	6.248	0.2857	893.		0.787	0.668	2232
		45.90	6.310	0.2896	914.		0.787	0.671	2081
		45.82	6.367	0.2917	929.		0.787	0.673	2231
		45.78	6.461	0.2958	956.		0.787	0.680	2219
		45.66	6.482	0.2960	959.		0.787	0.683	2230
		45.84	6.689	0.3066	1026.		0.787	0.690	2223
		45.90	6.742	0.3095	1043.		0.787	0.689	2227
		45.81	6.788	0.3109	1055.		0.787	0.684	2217
		46.66	6.740	0.3145	1060.		0.787	0.686	2026
		45.66	6.854	0.3130	1073.		0.787	0.683	2099
		45.74	6.879	0.3146	1082.		0.787	0.695	2229
		45.94	7.004	0.3218	1127.		0.787	0.683	2193
		45.85	7.043	0.3229	1137.		0.787	0.693	2228
		45.71	7.052	0.3223	1137.		0.787	0.693	2225
		45.68	7.135	0.3259	1163.		0.787	0.695	2166
		46.00	7.127	0.3279	1168.		0.787	0.688	2150
		45.88	7.140	0.3276	1170.		0.787	0.696	2096
		45.98	7.171	0.3297	1182.		0.787	0.690	2170
		46.20	7.183	0.3318	1192.		0.787	0.695	2172
		46.20	7.183	0.3318	1192.		0.787	0.687	2149
		45.80	7.255	0.3323	1205.		0.787	0.690	2148
		47.20	7.201	0.3399	1224.		0.787	0.700	2171
		45.88	7.317	0.3357	1228.		0.787	0.680	2174
		45.70	3.408	0.1557	265.		0.813	0.535	2745
		45.90	3.874	0.1778	344.		0.813	0.564	2757
		45.00	4.255	0.1915	407.		0.813	0.590	2743
		45.20	6.285	0.2841	893.		0.813	0.660	2721
		47.44	6.293	0.2985	939.		0.813	0.664	2055
		46.10	6.437	0.2968	955.		0.813	0.678	2628
		47.46	6.588	0.3127	1030.		0.813	0.676	2056
		45.00	7.010	0.3155	1106.		0.813	0.687	2724
		45.70	7.016	0.3207	1125.		0.813	0.680	2706
		45.70	7.062	0.3227	1140.		0.813	0.676	2705
		45.90	7.132	0.3274	1167.		0.813	0.682	2629
		45.66	7.227	0.3300	1192.		0.813	0.695	2175

PROJECTILE						BUMPER		ROUND NO.
MATERIAL	SIZE (CM)	MASS (MG)	VELOCITY (KM/SEC)	MOMENTUM (KGM/SEC)	ENERGY (JOULES)	MATERIAL	THICKNESS (MM)	HOLE DIA. (CM)	
ALUMINUM	0.317	46.00	7.202	0.3313	1193.	ALUMINUM	0.813	0.685	2661
		45.90	7.242	0.3324	1204.		0.813	0.682	2630
		45.70	7.260	0.3318	1204.		0.813	0.695	2659
		45.50	3.898	0.1774	346.		0.838	0.560	2553
		45.70	3.965	0.1812	359.		0.838	0.563	2552
		45.50	4.060	0.1847	375.		0.838	0.565	2737
		45.80	4.066	0.1862	379.		0.838	0.573	2554
		45.70	4.078	0.1864	380.		0.838	0.573	2758
		45.10	4.596	0.2073	476.		0.838	0.600	2738
		45.82	4.660	0.2135	498.		0.838	0.597	2559
		45.00	4.996	0.2248	562.		0.838	0.618	2739
		45.60	5.185	0.2364	613.		0.838	0.616	2782
		45.82	5.233	0.2398	627.		0.838	0.640	2382
		45.60	5.249	0.2393	628.		0.838	0.622	2768
		45.00	5.468	0.2461	673.		0.838	0.645	2735
		45.50	5.453	0.2481	676.		0.838	0.634	2764
		45.60	5.486	0.2502	686.		0.838	0.629	2770
		45.60	5.605	0.2556	716.		0.838	0.634	2773
		45.90	5.636	0.2587	729.		0.838	0.634	2788
		45.80	5.669	0.2597	736.		0.838	0.635	2761
		45.70	5.849	0.2673	782.		0.838	0.641	2783
		45.70	5.907	0.2700	797.		0.838	0.645	2794
		45.90	5.953	0.2732	813.		0.838	0.650	2790
		45.90	5.956	0.2734	814.		0.838	0.650	2792
		45.70	6.453	0.2949	951.		0.838	0.664	2759
		47.46	6.393	0.3034	970.		0.838	0.668	2054
		47.52	6.417	0.3049	978.		0.838	0.665	2053
		46.88	6.492	0.3044	988.		0.838	0.680	2037
		45.86	6.608	0.3030	1001.		0.838	0.668	2061
		46.75	6.550	0.3062	1003.		0.838	0.685	2023
		45.80	6.632	0.3038	1007.		0.838	0.668	2479
		46.72	6.584	0.3076	1013.		0.838	0.677	2033
		45.66	6.681	0.3051	1019.		0.838	0.667	2494
		47.46	6.581	0.3123	1028.		0.838	0.678	2043
		45.80	6.788	0.3109	1055.		0.838	0.674	2470
		45.82	6.797	0.3114	1058.		0.838	0.674	2467
		47.45	6.680	0.3170	1059.		0.838	0.668	2052
		45.78	6.879	0.3149	1083.		0.838	0.686	2389
		45.88	6.875	0.3154	1084.		0.838	0.688	2059

PROJECTILE						BUMPER			ROUND NO.
MATERIAL	SIZE (CM)	MASS (MG)	VELOCITY (KM/SEC)	MOMENTUM (KGM/SEC)	ENERGY (JOULES)	MATERIAL	THICKNESS (MM)	HOLE DIA. (CM)	
ALUMINUM	0.317	46.80	6.846	0.3204	1097.	ALUMINUM	0.838	0.703	2018
		45.79	6.925	0.3171	1098.		0.838	0.672	2370
		46.76	6.859	0.3207	1100.		0.838	0.688	2025
		45.97	6.925	0.3183	1102.		0.838	0.693	2381
		46.08	6.931	0.3194	1107.		0.838	0.672	2474
		47.54	6.843	0.3253	1113.		0.838	0.680	2050
		46.68	6.912	0.3226	1115.		0.838	0.693	2028
		47.56	6.848	0.3257	1115.		0.838	0.681	2044
		45.84	6.992	0.3205	1121.		0.838	0.700	2057
		47.10	6.915	0.3257	1126.		0.838	0.699	2015
		45.97	7.044	0.3238	1140.		0.838	0.691	2537
		45.80	7.074	0.3240	1146.		0.838	0.678	2344
		46.00	7.066	0.3250	1148.		0.838	0.690	2064
		46.00	7.074	0.3254	1151.		0.838	0.691	2535
		45.68	7.102	0.3244	1152.		0.838	0.678	2343
		45.88	7.101	0.3258	1157.		0.838	0.691	2063
		45.84	7.105	0.3257	1157.		0.838	0.695	2160
		45.82	7.111	0.3258	1158.		0.838	0.683	2361
		46.76	7.050	0.3297	1162.		0.838	0.685	2041
		45.70	7.163	0.3273	1172.		0.838	0.695	2398
		45.60	7.190	0.3279	1179.		0.838	0.675	2582
		45.70	7.212	0.3296	1188.		0.838	0.700	2545
		46.76	7.132	0.3335	1189.		0.838	0.691	2042
		45.89	7.205	0.3306	1191.		0.838	0.685	2062
		45.50	7.242	0.3295	1193.		0.838	0.687	2542
		45.72	7.230	0.3305	1195.		0.838	0.697	2400
		46.16	7.199	0.3323	1196.		0.838	0.697	2530
		45.80	7.230	0.3311	1197.		0.838	0.696	2399
		45.86	7.224	0.3313	1197.		0.838	0.682	2401
		45.73	7.257	0.3319	1204.		0.838	0.690	2372
		46.06	7.230	0.3330	1204.		0.838	0.680	2248
		47.54	7.127	0.3388	1207.		0.838	0.696	2047
		45.78	7.263	0.3325	1208.		0.838	0.681	2363
		45.30	7.306	0.3310	1209.		0.838	0.660	2581
		46.76	7.190	0.3362	1209.		0.838	0.681	2049
		46.00	7.254	0.3337	1210.		0.838	0.692	2402
		45.50	7.300	0.3321	1212.		0.838	0.677	2580
		45.60	7.294	0.3326	1213.		0.838	0.685	2583
		45.78	7.318	0.3350	1226.		0.838	0.696	2397
		45.90	7.376	0.3386	1249.		0.838	0.685	2601

PROJECTILE						BUMPER			ROUND NO.
MATERIAL	SIZE (CM)	MASS (MG)	VELOCITY (KM/SEC)	MOMENTUM (KGM/SEC)	ENERGY (JOULES)	MATERIAL	THICKNESS (MM)	HOLE DIA. (CM)	
ALUMINUM	0.317	46.76	7.326	0.3425	1255.	ALUMINUM	0.838	0.701	2040
		45.50	7.449	0.3389	1262.		0.838	0.690	2599
		47.56	7.312	0.3477	1271.		0.838	0.699	2046
		47.48	7.390	0.3509	1296.		0.838	0.701	2039
		46.50	6.518	0.3031	988.		0.864	0.688	2017
		46.70	7.228	0.3375	1220.		0.864	0.699	2036
		46.00	7.232	0.3327	1203.		1.041	0.753	2409
		45.74	7.266	0.3324	1208.		1.041	0.752	2407
		45.84	5.270	0.2416	637.		1.143	0.716	2561
		45.76	5.441	0.2490	677.		1.143	0.721	2560
		45.94	7.073	0.3250	1149.		1.168	0.800	2162
		45.85	6.992	0.3206	1121.		1.194	0.798	2140
		45.74	4.478	0.2048	459.		1.600	0.728	2556
		45.78	4.545	0.2081	473.		1.600	0.749	2236
		45.80	4.615	0.2114	488.		1.600	0.754	2558
		45.74	4.987	0.2281	569.		1.600	0.775	2557
		45.84	5.671	0.2600	737.		1.600	0.828	2073
		45.92	5.916	0.2717	804.		1.600	0.835	2111
		46.00	6.289	0.2893	910.		1.600	0.863	2104
		45.90	6.434	0.2953	950.		1.600	0.870	2105
		45.83	6.551	0.3002	984.		1.600	0.879	2060
		45.72	6.909	0.3159	1091.		1.600	0.899	2078
		45.65	6.968	0.3181	1108.		1.600	0.897	2058
		45.84	7.225	0.3312	1197.		1.600	0.911	2066
		46.00	7.223	0.3323	1200.		1.600	0.917	2095
		45.78	7.246	0.3317	1202.		1.600	0.909	2067
		45.74	7.267	0.3324	1208.		1.600	0.907	2068
		45.72	7.068	0.3232	1142.		1.626	0.934	2379
		45.64	3.972	0.1813	360.		1.702	0.702	2555
		45.82	5.267	0.2413	636.		2.540	0.934	2568
		45.76	5.428	0.2484	674.		2.540	0.944	2565

PROJECTILE						BUMPER		ROUND NO.
MATERIAL	SIZE (CM)	MASS (MG)	VELOCITY (KM/SEC)	MOMENTUM (KGM/SEC)	ENERGY (JOULES)	MATERIAL	THICKNESS (MM)	HOLE DIA. (CM)	
ALUMINUM	0.317	45.80	5.718	0.2619	749.	ALUMINUM	2.540	0.925	2562
		46.00	5.712	0.2627	750.		2.540	0.972	2564
		45.84	5.767	0.2644	762.		2.540	0.982	2563
		45.70	6.025	0.2753	829.		2.565	1.003	2072
		45.80	6.354	0.2910	925.		2.565	1.024	2080
		45.72	6.381	0.2917	931.		2.565	1.034	2071
		45.64	6.679	0.3048	1018.		2.565	1.054	2103
		45.82	6.879	0.3152	1084.		2.565	1.080	2077
		45.98	6.901	0.3173	1095.		2.565	1.085	2079
		45.70	7.262	0.3319	1205.		2.565	1.125	2069
		45.94	5.665	0.2603	737.		3.175	1.016	2083
		45.96	5.824	0.2677	779.		3.175	1.041	2084
		45.80	6.319	0.2894	914.		3.175	1.080	2082
		45.78	6.810	0.3118	1061.		3.200	1.153	2113
		45.76	6.649	0.3042	1011.		4.750	1.147	2102
		45.60	7.007	0.3195	1119.	TITANIUM	0.432	0.518	2143
		45.74	7.059	0.3229	1140.		0.432	0.515	2135
		45.94	7.070	0.3248	1148.		0.432	0.518	2136
		45.30	7.361	0.3334	1227.		0.432	0.512	2573
		45.89	6.861	0.3149	1080.		0.508	0.537	2438
		45.76	7.010	0.3208	1124.		0.508	0.534	2436
		45.84	7.010	0.3214	1126.		0.508	0.533	2437
		45.84	7.010	0.3214	1126.		0.508	0.541	2435
		45.75	6.904	0.3158	1090.		0.787	0.667	2165
		45.78	7.232	0.3311	1197.		0.787	0.670	2155
		45.80	7.104	0.3254	1156.		0.813	0.765	2137
		45.72	7.148	0.3268	1168.		0.838	0.670	2138
		45.68	7.174	0.3277	1176.		0.864	0.670	2181
		45.69	6.956	0.3178	1106.		1.168	0.740	2163

MATERIAL	SIZE (CM)	PROJECTILE MASS (MG)	VELOCITY (KM/SEC)	MOMENTUM (KGM/SEC)	ENERGY (JOULES)	MATERIAL	BUMPER THICKNESS (MM)	HOLE DIA. (CM)	ROUND NO.
ALUMINUM	0.317	45.86	6.683	0.3065	1024.	TITANIUM	1.194	0.740	2173
		46.03	6.930	0.3190	1105.		1.194	0.750	2154
		45.80	7.118	0.3260	1160.		1.194	0.753	2152
		45.86	7.173	0.3289	1180.		1.194	0.750	2153
		45.82	7.408	0.3394	1257.		1.194	0.758	2180
		45.68	6.742	0.3080	1038.	STEEL	0.076	0.336	2485
		45.76	6.855	0.3137	1075.		0.076	0.334	2488
		45.84	6.870	0.3149	1082.		0.076	0.337	2487
		46.04	6.971	0.3209	1119.		0.076	0.337	2486
		46.14	7.007	0.3233	1133.		0.076	0.336	2489
		45.76	7.007	0.3207	1123.		0.203	0.443	2411
		45.80	7.059	0.3233	1141.		0.203	0.442	2410
		45.80	7.202	0.3299	1188.		0.305	0.497	2345
		45.92	7.007	0.3218	1127.		0.381	0.531	2413
		46.00	7.026	0.3232	1135.		0.381	0.543	2414
		45.76	7.102	0.3250	1154.		0.381	0.538	2412
		45.66	6.959	0.3177	1105.		0.660	0.627	2442
		46.35	6.888	0.3193	1100.	CADMIUM	0.102	0.397	2431
		45.84	6.980	0.3200	1117.		0.102	0.410	2434
		45.83	7.010	0.3213	1126.		0.102	0.387	2430
		45.72	7.197	0.3290	1184.		0.102	0.395	2432
		48.81	7.081	0.3456	1224.		0.102	0.387	2433
		45.76	6.971	0.3190	1112.		0.178	0.476	2421
		45.90	7.120	0.3268	1163.		0.178	0.468	2420
		45.80	7.163	0.3281	1175.		0.178	0.472	2419
		45.78	6.849	0.3135	1074.		0.279	0.551	2493
		45.49	6.931	0.3153	1093.		0.279	0.547	2415
		45.70	7.050	0.3222	1136.		0.381	0.650	2416
		45.79	7.141	0.3270	1168.		0.381	0.660	2417
		45.75	6.971	0.3189	1112.		0.508	0.785	2423

MATERIAL	SIZE (CM)	PROJECTILE MASS (MG)	VELOCITY (KM/SEC)	MOMENTUM (KGM/SEC)	ENERGY (JOULES)	MATERIAL	BUMPER THICKNESS (MM)	HOLE DIA. (CM)	ROUND NO.
ALUMINUM	0.317	46.12	6.736	0.3107	1046.	CADMIUM	0.838	0.995	2480
		45.74	6.986	0.3195	1116.		0.838	0.975	2422
		45.80	7.068	0.3237	1144.		0.838	0.945	2440
		46.00	6.739	0.3100	1045.	NICKEL	0.279	0.502	2483
		45.82	6.797	0.3114	1058.		0.279	0.502	2482
		45.79	6.922	0.3170	1097.		0.279	0.500	2481
		45.78	6.971	0.3191	1112.	COPPER	0.279	0.529	2425
		45.73	7.056	0.3227	1138.		0.279	0.530	2424
		46.09	7.065	0.3256	1150.		0.279	0.529	2429
		45.80	6.940	0.3179	1103.		0.406	0.595	2144
		45.82	6.984	0.3200	1118.		0.406	0.600	2145
		45.90	6.856	0.3147	1079.		0.787	0.801	2114
		45.86	7.153	0.3281	1173.		0.787	0.805	2182
		45.84	7.269	0.3332	1211.		0.787	0.804	2151
		45.88	6.925	0.3177	1100.		0.813	0.795	2139
		45.92	6.983	0.3207	1120.		0.813	0.802	2133
		45.76	7.041	0.3222	1134.		0.813	0.803	2117
		45.78	6.633	0.3037	1007.		0.838	0.788	2305
		45.75	7.075	0.3237	1145.		0.838	0.800	2161
		45.86	6.919	0.3173	1098.		1.143	0.897	2142
		45.70	7.152	0.3269	1169.		1.143	0.913	2141
		45.70	7.044	0.3219	1134.		1.600	0.998	2569
		45.84	7.129	0.3268	1165.	LEAD	0.203	0.542	2356
		45.54	7.227	0.3291	1189.		0.203	0.544	2349
		45.76	7.236	0.3311	1198.		0.203	0.545	2358
		45.76	7.251	0.3318	1203.		0.203	0.548	2350
		45.86	7.266	0.3332	1211.		0.203	0.567	2351
		45.90	7.145	0.3279	1171.	TANTALUM	0.127	0.439	2348
		45.84	7.163	0.3283	1176.		0.127	0.440	2353
		45.65	7.215	0.3293	1188.		0.127	0.442	2364

PROJECTILE						BUMPER			ROUND NO.
MATERIAL	SIZE (CM)	MASS (MG)	VELOCITY (KM/SEC)	MOMENTUM (KGM/SEC)	ENERGY (JOULES)	MATERIAL	THICKNESS (MM)	HOLE DIA. (CM)	
ALUMINUM	0.317	45.86	7.401	0.3394	1256.	TANTALUM	0.127	0.443	2347
		45.86	7.015	0.3217	1128.	TUNGSTEN	0.152	0.427	2124
	0.635	373.30	5.544	2.0697	5738.	ALUMINUM	1.575	1.235	2591
		372.60	6.541	2.4372	7971.		1.575	1.380	2598
		372.90	6.745	2.5153	8483.		1.600	1.344	2715
		374.20	6.943	2.5982	9020.		1.600	1.337	2625
		373.00	6.983	2.6046	9094.		1.600	1.349	2714
		373.90	7.013	2.6223	9196.		1.600	1.348	2623
		373.20	7.026	2.6220	9211.		1.600	1.349	2655
		373.20	7.096	2.6481	9395.		1.600	1.362	2654
		373.20	7.132	2.6618	9492.		1.600	1.349	2660
		373.90	7.221	2.6998	9747.		1.600	1.374	2622
		374.30	7.355	2.7529	10124.		1.600	1.358	2627
		374.30	6.358	2.3798	7566.		3.175	1.368	2624
STEEL	0.317	129.10	7.113	0.9183	3266.	STEEL	0.635	0.643	2190
		129.30	6.666	0.8619	2873.	COPPER	0.813	0.820	2680
CADMIUM	0.317	152.40	6.096	0.9290	2832.	CADMIUM	0.813	0.975	2637
		146.50	6.581	0.9641	3172.		0.813	0.950	2674
		147.10	6.856	1.0085	3457.		0.813	0.925	2679
		150.10	6.943	1.0422	3618.		0.813	0.926	2675
		147.10	7.041	1.0357	3646.		0.813	0.942	2716
		151.20	7.004	1.0591	3709.		0.813	0.953	2682
		152.70	6.998	1.0686	3739.		0.813	0.979	2636
		151.50	7.056	1.0690	3772.		0.813	0.960	2635
		147.50	7.160	1.0561	3781.		0.813	1.024	2662
		151.80	7.059	1.0716	3782.		0.813	1.050	2633
		153.00	7.074	1.0824	3829.		0.813	1.000	2634
		151.90	7.129	1.0829	3860.		0.813	0.965	2657
		149.50	7.187	1.0745	3861.		0.813	0.955	2710
		154.70	7.071	1.0939	3868.		0.813	0.951	2664
		155.60	7.113	1.1068	3937.		0.813	0.975	2666

PROJECTILE						BUMPER			ROUND NO.
MATERIAL	SIZE (CM)	MASS (MG)	VELOCITY (KM/SEC)	MOMENTUM (KGM/SEC)	ENERGY (JOULES)	MATERIAL	THICKNESS (MM)	HOLE DIA. (CM)	
CADMIUM	0.317	149.50	7.282	1.0886	3963.	CADMIUM	0.813	0.975	2672
		153.69	6.657	1.0231	3405.		0.838	0.922	2469
		153.60	6.721	1.0323	3469.		0.838	0.990	2473
		152.40	6.782	1.0335	3505.		0.838	0.963	2497
		156.76	6.757	1.0593	3579.		0.838	0.973	2466
		151.80	6.886	1.0453	3599.		0.838	0.980	2118
		149.60	6.936	1.0376	3595.		0.838	0.950	2125
		156.40	6.879	1.0759	3701.		0.838	0.947	2426
		151.80	7.001	1.0628	3720.		0.838	0.954	2617
		153.50	7.029	1.0789	3792.		0.838	0.950	2427
		152.50	7.056	1.0761	3796.		0.838	0.986	2595
		150.78	7.141	1.0768	3845.		0.838	0.980	2403
		152.80	7.111	1.0866	3863.		0.838	0.959	2606
		156.50	7.053	1.1038	3893.		0.838	1.000	2406
		152.70	7.163	1.0938	3917.		0.838	0.940	2538
		152.00	7.778	1.1823	4598.		0.838	0.975	2602
		151.80	3.195	0.4843	774.		1.575	1.078	2214
		148.00	6.703	0.9920	3324.		1.575	1.423	2199
COPPER	0.317	152.20	6.902	1.0505	3625.	ALUMINUM	0.787	0.658	2119
		153.80	6.992	1.0754	3760.	COPPER	0.381	0.579	2579
		150.00	7.123	1.0685	3805.		0.381	0.546	2574
		150.60	7.193	1.0833	3896.		0.381	0.535	2575
		155.20	7.495	1.1632	4359.		0.381	0.572	2577
		152.30	6.518	0.9926	3235.		0.787	0.818	2108
		152.20	6.825	1.0387	3545.		0.787	0.835	2120
		152.80	6.841	1.0453	3575.		0.787	0.835	2178
		152.70	7.061	1.0782	3807.		0.787	0.843	2183
		154.70	6.440	0.9963	3208.		0.813	0.855	2648
		148.60	6.590	0.9792	3226.		0.813	0.827	2708
		156.00	6.553	1.0223	3350.		0.813	0.844	2632
		155.14	6.660	1.0332	3441.		0.813	0.832	2465
		144.30	7.044	1.0164	3580.		0.813	0.820	2646
		160.70	6.681	1.0737	3587.		0.813	0.832	2644

MATERIAL	SIZE (CM)	PROJECTILE MASS (MG)	VELOCITY (KM/SEC)	MOMENTUM (KGM/SEC)	ENERGY (JOULES)	MATERIAL	BUMPER THICKNESS (MM)	HOLE DIA. (CM)	ROUND NO.
COPPER	0.317	152.50	6.943	1.0588	3676.	COPPER	0.813	0.846	2128
		150.10	7.010	1.0523	3688.		0.813	0.851	2673
		153.80	6.928	1.0655	3691.		0.813	0.858	2717
		163.50	6.767	1.1063	3743.		0.813	0.833	2631
		154.00	6.983	1.0754	3755.		0.813	0.818	2678
		158.40	6.983	1.1061	3862.		0.813	0.825	2709
		161.70	7.099	1.1479	4074.		0.813	0.830	2649
		159.90	7.169	1.1463	4109.		0.813	0.843	2671
		164.30	7.129	1.1713	4175.		0.813	0.860	2668
		150.22	5.215	0.7834	2043.		0.838	0.757	2377
		155.94	6.401	0.9981	3194.		0.838	0.841	2388
		148.75	6.651	0.9893	3290.		0.838	0.835	2383
		156.70	6.596	1.0336	3409.		0.838	0.830	2495
		153.17	6.776	1.0378	3516.		0.838	0.830	2471
		148.22	6.898	1.0224	3526.		0.838	0.830	2375
		157.93	6.745	1.0653	3593.		0.838	0.843	2475
		148.75	6.953	1.0343	3596.		0.838	0.863	2380
		156.89	6.815	1.0693	3644.		0.838	0.825	2472
		157.93	6.843	1.0807	3697.		0.838	0.829	2468
		148.74	7.062	1.0504	3709.		0.838	0.831	2394
		154.20	6.959	1.0730	3733.		0.838	0.830	2543
		147.60	7.132	1.0527	3754.		0.838	0.869	2365
		147.60	7.145	1.0545	3767.		0.838	0.835	2357
		148.70	7.126	1.0597	3776.		0.838	0.860	2593
		149.40	7.114	1.0628	3781.		0.838	0.842	2352
		151.00	7.138	1.0779	3847.		0.838	0.851	2393
		151.60	7.145	1.0831	3869.		0.838	0.828	2335
		149.84	7.196	1.0783	3880.		0.838	0.878	2367
		156.60	7.047	1.1036	3888.		0.838	0.890	2544
		150.20	7.196	1.0809	3889.		0.838	0.859	2362
		155.20	7.093	1.1008	3904.		0.838	0.825	2532
		153.50	7.163	1.0995	3938.		0.838	0.832	2395
		152.40	7.196	1.0967	3946.		0.838	0.867	2392
		155.10	7.166	1.1114	3982.		0.838	0.808	2536
		151.40	7.266	1.1001	3997.		0.838	0.847	2338
		153.50	7.254	1.1135	4039.		0.838	0.843	2396
		157.30	7.248	1.1401	4132.		0.838	0.840	2611
		160.80	7.175	1.1537	4139.		0.838	0.857	2600
		160.40	7.212	1.1567	4171.		0.838	0.855	2592

PROJECTILE						BUMPER			ROUND NO.
MATERIAL	SIZE (CM)	MASS (MG)	VELOCITY (KM/SEC)	MOMENTUM (KGM/SEC)	ENERGY (JOULES)	MATERIAL	THICKNESS (MM)	HOLE DIA. (CM)	
COPPER	0.317	160.00	7.239	1.1582	4192.	COPPER	0.838	0.840	2603
		157.90	7.532	1.1892	4478.		0.838	0.840	2594
		132.30	4.455	0.5894	1313.		1.575	0.943	2205
		143.60	6.506	0.9343	3039.		1.575	1.008	2209
		135.30	6.807	0.9210	3135.		1.575	1.130	2201
		139.10	6.773	0.9421	3190.		1.575	1.139	2198
		148.10	6.904	1.0224	3529.		1.600	1.168	2374
		153.70	7.126	1.0953	3903.		1.600	1.162	2570

Unclassified
Security Classification

DOCUMENT CONTROL DATA - R & D

(Security classification of title, body of abstract and indexing annotation must be entered when the overall report is classified)

1. ORIGINATING ACTIVITY (Corporate author)	2a. REPORT SECURITY CLASSIFICATION
University of Dayton Research Institute 300 College Park Avenue Dayton, Ohio 45409	Unclassified 2b. GROUP

3. REPORT TITLE

HOLE GROWTH IN THIN PLATES PERFORATED BY HYPERVELOCITY PELLETS

4. DESCRIPTIVE NOTES (Type of report and inclusive dates)

Technical Report

5. AUTHOR(S) (First name, middle initial, last name)

W. C. Turpin
Capt. J. M. Carson, USAF

6. REPORT DATE	7a. TOTAL NO. OF PAGES	7b. NO. OF REFS
April 1970	47	12

8a. CONTRACT OR GRANT NO.	9a. ORIGINATOR'S REPORT NUMBER(S)
F33615-68-C-1138 b. PROJECT NO. 7360 c. Task No. 736006 d.	UDRI-TR-70-16 9b. OTHER REPORT NO(S) (Any other numbers that may be assigned this report) AFML-TR-70-83

10. DISTRIBUTION STATEMENT

This document has been approved for public release and sale; its distribution is unlimited.

11. SUPPLEMENTARY NOTES	12. SPONSORING MILITARY ACTIVITY
	Air Force Materials Laboratory Air Force Systems Command Wright-Patterson AFB, Ohio 45433

13. ABSTRACT

An experimental study has measured hole growth rates in thin plates impacted by hypervelocity pellets. These hole growth rates were obtained for 0.85 mm thick plates made of aluminum, copper, and cadmium impacted at 5-7 km/sec with 3.18 mm spheres of like material. The growth process was found to be a two stage process. Results are compared with the numerical predictions from a two dimensional impact code. These dynamic results are combined with observations resulting from a catalog of over 400 hole corpse measurements to form a qualitative model of thin plate impact.

DD FORM 1 NOV 65 1473

Unclassified
Security Classification

14. KEY WORDS	LINK A		LINK B		LINK C	
	ROLE	WT	ROLE	WT	ROLE	WT
Impact						
Hypervelocity Impact						
Thin Plates						
Perforation						
Hole Formation						